The Meteoritical Society

Meteoritics & Planetary Science 57, Nr 11, 2081–2101 (2022)
doi: 10.1111/maps.13913

Malotas (b), a new eucrite from an old fall

Marcela E. SAAVEDRA[1]*, Julia ROSZJAR[2], My E. I. RIEBE[3], María E. VARELA[1], Shuying YANG[4], Munir HUMAYUN[4], Ryoji TANAKA[5], and H. BUSEMANN[3]

[1]ICATE-CONICET, Av. España 1512 Sur, San Juan J5402DSP, Argentina
[2]Department of Mineralogy and Petrography, Natural History Museum Vienna, Burgring 7, 1010 Vienna, Austria
[3]Department of Earth Sciences, Institute of Geochemistry and Petrology, ETH Zürich, 8092 Zürich, Switzerland
[4]National High Magnetic Field Laboratory and Department of Earth, Ocean and Atmospheric Science, Florida State University, Tallahassee, Florida 32310, USA
[5]Institute for Planetary Materials, Okayama University, 827 Yamada, Misasa, Tottori 682-0193, Japan
*Corresponding author. E-mail: m.saavedra@conicet.gov.ar

(Received 23 February 2022; revision accepted 09 August 2022)

Abstract–On the night of June 22, 1931 at 4 h 30 min, a fireball was seen in the vicinity of Malotas, Argentina. During the atmospheric trajectory (southwest to northeast), it experienced several fragmentation events. After the fall, a piece was given to Professor Juan A. Olsacher (National University of Córdoba City, Argentina), who collected some further pieces. One of those samples was officially classified as an H5 ordinary chondrite termed Malotas. The present work focuses on the study of another two pieces rediscovered recently in the Museo de Mineralogía y Geología Dr. Alfred Stelzner in Cordoba City, Argentina. The first piece turned out to be an achondritic meteorite termed Malotas (b). Petrographic features, chemical composition, and oxygen isotopes point to a monomict basaltic eucrite belonging to the Stannern-trend chemical subgroup of eucrites. The occurrence of anorthitic plagioclase veins in clinopyroxene, veinlet apatite, irregular-shaped pockets of silica and troilite and porous silica signal metasomatism and thermal annealing before a late thermal event took place after brecciation. The latter was possibly recorded in the nominal U/Th-^{4}He ages of 1.2–3.4 Ga detected in this work, whereas nominal K-Ar gas retention ages are within the range 3.5–4.2 Ga and may have escaped late thermal modifications. The second piece is classified as an L5 chondrite. The different cosmic ray exposure ages of 3, ~50, and 27 Ma determined for the H5 and L5 chondrites and the eucrite samples, respectively, might signal a common fall as a result of the breakup of a polymict meteoroid.

INTRODUCTION

The HED (howardite–eucrite–diogenite) clan of meteorites represents the largest group of achondrites and provides an unmatched look at differentiation processes that occurred on asteroidal-sized bodies (Mittlefehldt, 2015). Their uniform oxygen isotope composition, with only few exceptions, points toward a single parent body (e.g., Greenwood et al., 2005, 2017; McSween et al., 2011). Based on the similarity of reflectance spectra between howardites, eucrites, and diogenites and the surface materials on the asteroid 4 Vesta, the HED meteorites are considered to have originated from 4 Vesta (e.g., Binzel & Xu, 1993; Consolmagno & Drake, 1977; Drake, 2001; McCord et al., 1970; McSween et al., 2011, 2013; Mittlefehldt, 2015; Russell et al., 2012; Thomas et al., 1997). The HED clan is a complex suite of crustal, mafic, and ultramafic rocks. Eucrites are pigeonite–plagioclase basalts composing the largest suite of rocks and are some of the most ancient basalts in the solar system formed 4.46–4.56 Gyr ago (e.g., Nyquist et al., 1986). Diogenites are ultramafic rocks mainly composed of orthopyroxene and olivine (e.g., Beck & McSween, 2010; Mittlefehldt et al., 1998) and howardites are polymict breccias defined as having >10% of a mixture

of diogenite and eucrite material (e.g., Buchanan et al., 2000; Buchanan & Mittlefehldt, 2003; Mittlefehldt, 1979).

Although eucrites can be unbrecciated, most basaltic eucrites are fragmental breccias composed of one or several different lithologies (monomict or polymict, respectively) that have undergone varying degrees of thermal metamorphism. Most brecciated eucrites consist of approximately 40% by weight of plagioclase and 60% of pyroxene (Consolmagno & Drake, 1977). The chemical composition of eucrites points toward a formation process similar to that of terrestrial basalts, gabbros, and diabases (Barrat et al., 2007; Duke & Silver, 1967; Mason, 1962). However, they have lower contents of volatile elements and contain minor metallic iron. Their magmatic textures are considered to represent one of the earliest planetary igneous activities of a differentiated asteroidal parent body (Binzel & Xu, 1993; Consolmagno & Drake, 1977; Drake, 2001; Mittlefehldt et al., 2013; Reddy et al., 2012). Only a few eucrites (e.g., Elephant Moraine [EET] 90020, Caldera, Ibitira, Pasamonte) display unusual petrographic features and distinct oxygen isotopic compositions and could therefore have originated from distinct parent bodies (e.g., Bland et al., 2009; Scott et al., 2009; Yamaguchi et al., 2002).

As of July 2022, according to the Meteoritical Bulletin Database (https://www.lpi.usra.edu/meteor/metbull.php), there are 2636 records of HED meteorites including 70 falls (=2.7%) of all HED meteorites listed, with a total of 40 eucrites among them and only four of them being confirmed falls (https://www.lpi.usra.edu/meteor/metbull.php), including two impact craters, that is Campo del Cielo and Rio Cuarto, and nine pseudo- or doubtful meteorites. The newly rediscovered (see next paragraph) eucrite Malotas (b) is the fifth Argentinian eucrite and only the third with an associated fall event, which is further discussed here together with its petrographic features, bulk chemical and oxygen isotopic composition, and cosmic ray exposure (CRE) ages. Preliminary data on this meteorite have been previously presented by Saavedra et al. (2019). Other more recent records of observed eucrite falls include the Puerto Lápice eucrite in Spain 2007 (Llorca et al., 2009), the Serra Pelada eucrite in Brazil in 2017 (Zucolotto et al., 2018), and Motopi Pan HED polymict breccia 2018 in Botswana that is connected to the asteroid 2018 LA and likely originated from 4 Vesta (Jenniskens et al., 2021).

Historical Aspects Related to the Fall

In 1931, rock samples of a recent observed meteorite fall in Santiago del Estero, Argentina, were given to Professor Juan A. Olsacher from Córdoba University, Argentina, who decided to inspect the fall locality and collect some further pieces. His report indicates that the fall covered an area of 5 × 2.5 km with the main axis having a southwest to northeast direction in the vicinity of the Dulce River (Olsacher, 1931). As the area was covered by a dense forest, he was able to collect three pieces only. Thus, it is likely that many individual pieces remained unrecovered. His studies showed that the meteorite is made up of fragments that correspond to two different types based on their composition and structure: one is chondritic [classified as an H5], composed by olivine and pyroxene with abundant metallic minerals; the second one is feldspar-rich with scarce presence of the previous components and with an ophitic texture [i.e., achondritic]. This fact and the circumstance that no fragment has been found so far that participates in both compositions leads us to think that they belong to two areas or mantles of the star of origin of well-defined differences and that therefore they must have occupied in these places far from each other. This speaks in favor of the idea that this meteorite has already been, before entering the Earth's atmosphere, not a single block shattered during its course through it, but a set of fragments. Helping to support this supposition is the fact that there are surfaces whose characters reveal that they correspond to fractures produced during their passage through the air, shortly before falling, since the thickness of the layer altered by the high temperature is very small while the surfaces that surround the fragments in almost all their extension, except the corresponding parts. These fractures present a calcined layer half a millimeter thick, the formation of which has required a longer contact with the atmosphere… According to the data collected, the distribution field of these fragments has a length of five kilometers and a width of two and a half kilometers, with its major axis coinciding with the course of the meteorite's trajectory. According to the same references, larger pieces are found on the east bank of the Río Dulce, according to the general fact that in the distribution fields of these rain of stones the largest fragments are found in the zone opposite the direction of their trajectory for being the first to fall. The thick jungle that covers the region where the meteorite has fallen is a great obstacle to the search for its fragments as well as to establish its distribution according to size, but it is possible to calculate their number in some thousands. (For details see Data S2 in supporting information) Accordingly, and due to the lack of enough bibliography at that time, he decided to leave the description of the achondritic meteorite for a complementary report. However, there are no records of such a report.

Circumstances of the Recovery of the Studied Samples

During a visit to the small meteorite collection of the Museo de Mineralogía y Geología Dr. Alfred Stelzner in Cordoba City, one of us (M.E.V.) found that two different stones (a chondrite and an achondrite) were exhibited in the showcase, labeled as "Malotas, 1931." Recognizing that one of the stones was not an ordinary chondrite, we made a detailed study of both stones. The ordinary chondrite termed Malotas (c) has a total mass of 79.4 g. A petrographic study of two thin sections revealed the occurrence of relict fragments and chondrules with minimal shock features, for example, faint undulatory extinction and absence of planar fractures. Major element analysis of the main mineral phases was measured by employing electron probe microanalysis (EPMA). The chemical compositions of olivine ($Fa_{24.56}$) and pyroxene ($Fs_{21.17}$; $Wo_{1.47}$), are consistent with an L group chondrite, petrological type 5. Malotas was officially classified as an H5 chondrite based on Malotas' chemical composition of olivine Fa_{19} (Mason, 1963), with a Co concentration of 1100 μg g^{-1} (Lingner et al., 1987), and a magnetic susceptibility of 5.40. The main mass of Malotas (4712 g) is in the private collection of E. Jawerbaum (Buenos Aires), who generously provided new fragments from which our petrological and chemical studies corroborated the classification as an H5 group chondrite. Therefore, having two chondritic fragments, the H5 Malotas and L5 Malotas (c) and the eucrite Malotas (b), a crucial question arises: Is Malotas a polymict fall?

Here, a petrologic, chemical, and O isotope study is carried out on Malotas (b) jointly with a CRE age study of the two ordinary H5 and L5 chondrites together with Malotas (b) to (re)evaluate the 1931 fall.

SAMPLES AND ANALYTICAL TECHNIQUES

Samples

The Malotas (b) samples prepared for this study include four thin sections and two thick polished sections in total (O2367 polished section and O2368 polished thin section at NHM Vienna and Malotas [b] 1-2-3-4 from Icate collection). Macroscopically, Malotas (b) is an individual piece with an original weight of 62.4 g. The interior is very fresh and covered by a very shiny black fusion crust (Fig. 1). The main mass remains in the meteorite collection of the Museo de Mineralogía y Geología Dr. Alfred Stelzner (Córdoba, Argentina).

Analytical Techniques

Detailed analytical procedures used to describe the Malotas (b) sample are provided in the supporting information (See Data S1).

RESULTS

Petrography

Underneath the very thin and shiny black fusion crust, the interior of Malotas (b) (Fig. 1) looks very fresh with a heterogeneous, brecciated appearance. It shows two distinct textures with different grain sizes: FG and CG lithology areas. The CG portions are composed of mineral clasts and lithic fragments set in a FG fragmental matrix (Fig. 2a). Optical microscopy and electron microscopy reveal that both the CG and FG areas are composed of similar silicate phases and mineral chemical compositions inferring a monomict nature of this meteorite (Tables S1 and S2). The main silicate phases are low-Ca pyroxene, high-Ca pyroxene, and plagioclase. Minor phases include chromite, ilmenite, F-apatite, merrillite, silica, troilite, and zircon, with typical sizes in the range of ~6 × 20 μm.

The CG lithology exhibits an ophitic–subophitic texture characterized by abundant anhedral pyroxene grains ranging in size between 500 μm and 1 mm. They show well-developed exsolution lamellae (Fig. 2b) of variable thicknesses (from less than 1 to ~10 μm) and contain abundant small mineral inclusions. These inclusions are predominantly chromite, ilmenite, plagioclase, troilite, and (veinlet) F-apatite (Fig. 2c). In addition to pyroxene, the CG lithology contains roughly equidimensional anhedral to subhedral plagioclase (>500 μm across) which exhibits undulatory extinction. Occasionally, plagioclase can contain numerous pyroxene inclusions of <5 μm (Fig. 2d). Plagioclase veinlets are also observed mainly infilling fractures in pyroxene as well as occurring along edge grains (Fig. 2e). Silica is abundant in the CG portion of the rock in a clear contact with pyroxene and plagioclase grains.

The FG lithology is characterized by roughly equidimensional anhedral to subhedral pyroxene and plagioclase grains. The matrix has an average grain size of ~120 μm (Fig. 2b). Some pyroxene and plagioclase grains develop a granoblastic texture with equidimensional polygonal crystals indicating that at least part of the rock underwent a stage of recrystallization (Fig. 2f).

Opaque minerals including zircon, troilite, ilmenite, and chromite are found in both lithologies but with different sizes and abundances. In the CG lithology, opaque minerals are larger (few to hundred microns) than in the FG lithology and occupy interstices between

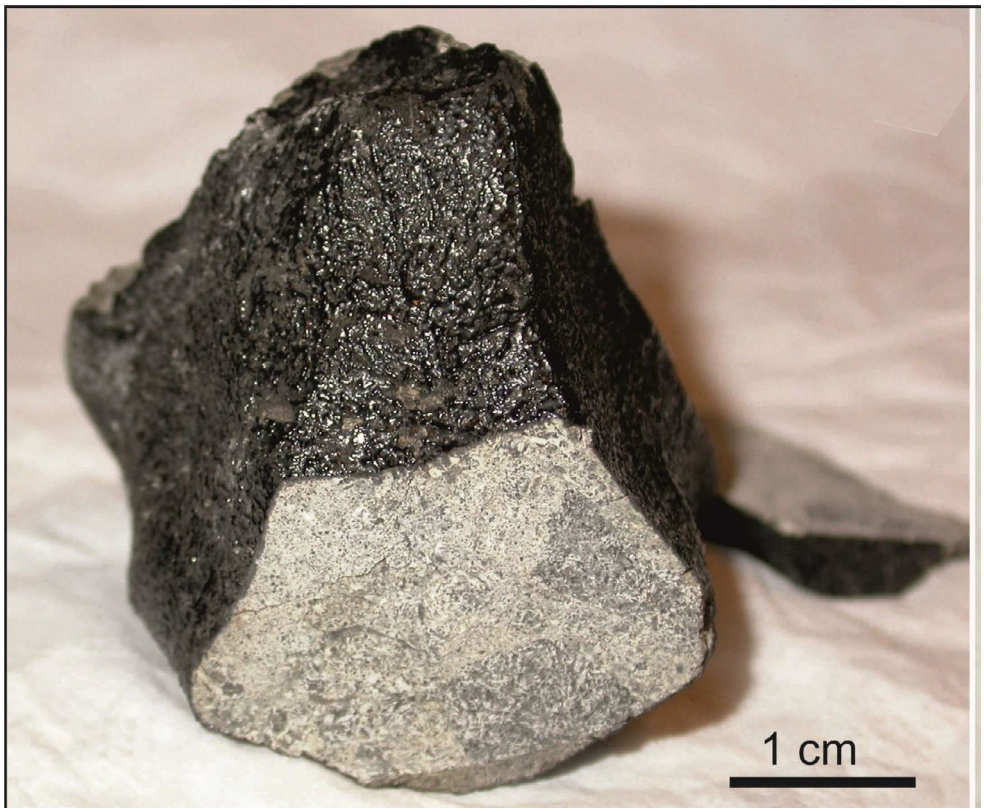

Fig. 1. Cut section of the Malotas (b) eucrite from the collection of the Museo de Mineralogía y Geología Dr. Alfred Stelzner in Cordoba, Argentina. The full sample photograph shows the relatively constant thickness of the fusion crust (~0.1 mm) completely enclosing the fresh, light gray sample. (Color figure can be viewed at wileyonlinelibrary.com.)

silicate minerals. Frequently, ilmenite and chromite occur as individual grains and/or grain aggregates with subhedral to anhedral morphologies reaching up to ~100 μm in size (Fig. 3a). Small inclusions of plagioclase and zircon are present inside ilmenite (Fig. 3b).

Fluor-apatite is slightly more abundant in the CG portion, whereas merrillite, typically <30 μm and highly fractured, is more common in the FG portion (Fig. 3c).

Shock Veins

We have identified a large shock melt vein with a glassy texture that cuts across the coarse and fine lithologies (Fig. 3d). It is elongated in shape (~1.2 cm long; 5–50 μm wide) and exhibits a pronounced Schlieren-like texture containing abundant troilite droplets that are usually <5 μm in apparent diameter (Fig. 3d).

Veinlets Inside Silicates

The veinlets in Malotas (b) are mainly composed of anorthitic plagioclase ($An_{96.1\pm1.4}$; Table S1) and F-apatite (Table S1) and are observed inside large pyroxene grains (≥500 μm in width). They are irregular with thicknesses that vary between 10 and 20 μm in size; a few examples of anorthite veins are shown in Fig. 2c. The lack of similar veinlets in other mineral phases shows that they are restricted to the large pyroxene grains in which they occur along pre-existing fractures and crystallographic cleavage planes.

Bulk Chemical Composition

Estimates of percentages of the FG and CG portions in the sample were performed using ImageJ software, a public domain software for processing and analyzing scientific images. After calculating the contribution of each lithology to the total area of the image, the program counts and measures objects in "binary," black and white, images. The estimated percentages of the CG and FG are 53% and 47%, respectively. Therefore, the bulk chemical composition is adjusted to these percentages.

Both portions have nearly identical chemical composition with Mg# of 38 and FeO_T/MnO of 33–34 (Table S3). The CG portion has higher TiO_2 (1.3 versus 0.6 wt%), P_2O_5 (0.18 versus 0.07 wt%), and sulfur (0.45 versus 0.08 wt%) and lower Cr_2O_3 (0.33 versus 0.40 wt %) as compared to the FG portion. Concentration of

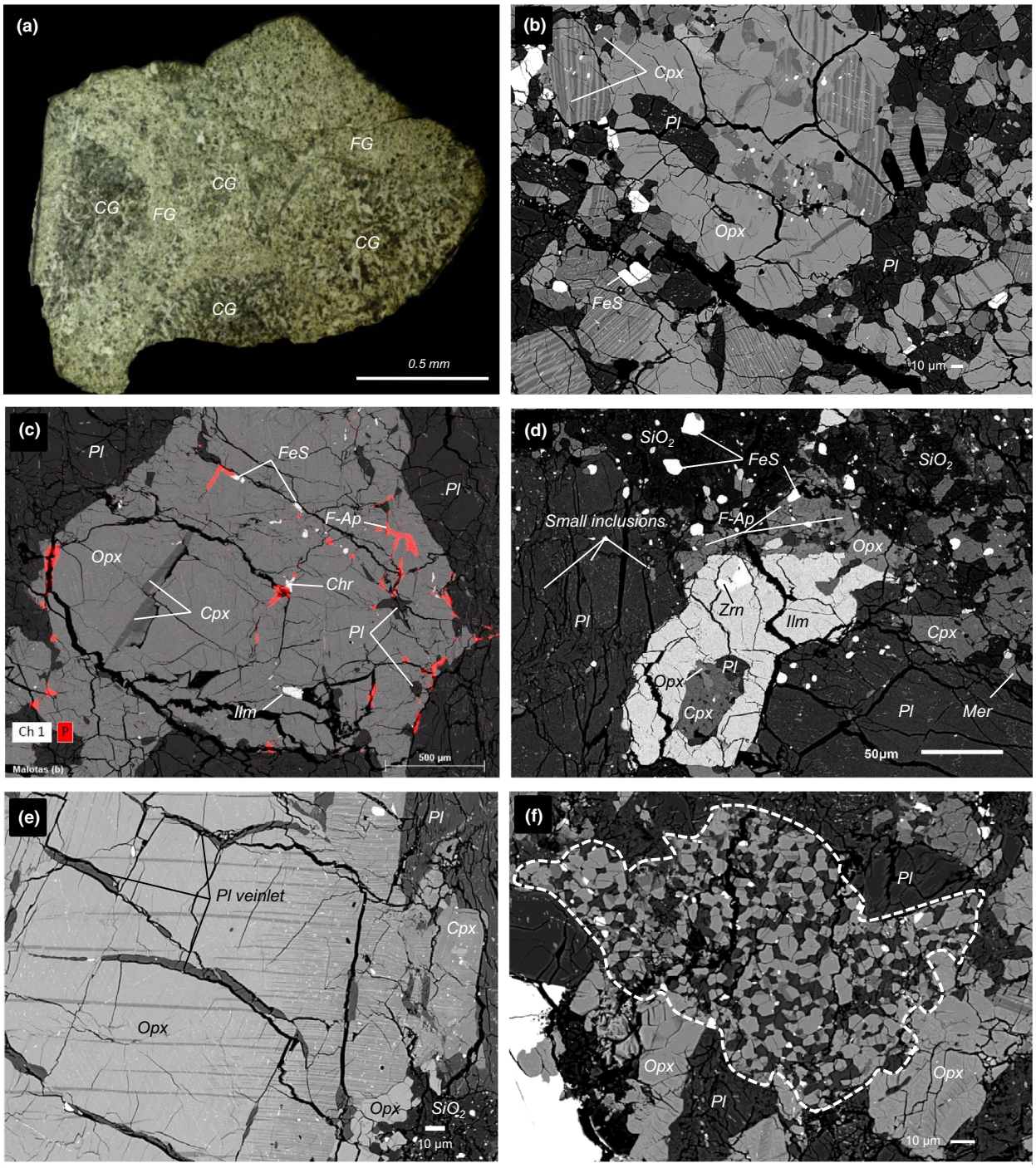

Fig. 2. a) Photomosaic of the polished thick section of Malotas (b) showing the coarse (CG)- and fine-grained (FG) lithic portions. b) Backscatter electron (BSE) image of orthopyroxene (Opx) grains with clinopyroxene (Cpx) exsolution lamellae of variable thicknesses (from less than 1 to ~10 µm) and plagioclase (Pl). c) BSE image with superimposed SEM EDS P-map showing a detail from Opx grain (size ~500 µm) with abundant inclusions, including chromite (Chr), ilmenite (Ilm), plagioclase (Pl), troilite (FeS), and Cpx exsolution. The Opx also contains fluorapatite (F-Ap) veinlets (indicated in red P map) within pre-existing fractures and crystallographic cleavage planes. d) BSE image showing the heterogeneous distribution of small inclusions in plagioclase grains; relatively large Ilm grain with enclosed zircon (Zrn) associated with Opx, Cpx, Pl, F-Ap, merrillite (Mer), and silica (SiO_2) with abundant FeS inclusions. e) Detailed BSE image showing the network of plagioclase veinlets percolating through a large pyroxene grain with exsolution lamellae. f) BSE image with details from the outlined recrystallized area in the FG lithology (a), composed of equidimensional polygonal crystals of Pl and Opx. (Color figure can be viewed at wileyonlinelibrary.com.)

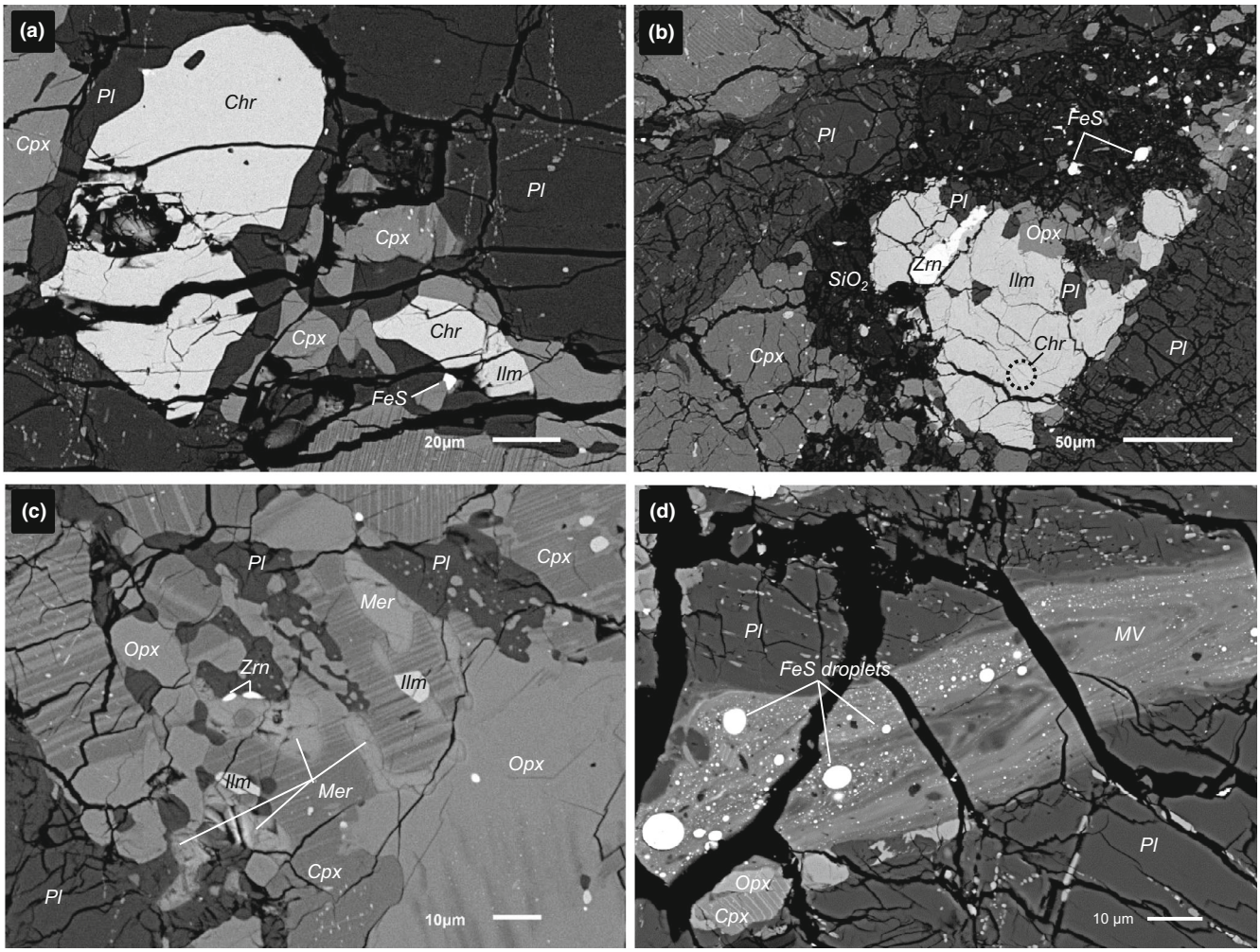

Fig. 3. BSE images of major and minor phases in Malotas (b). a) Chromite (Chr) occurs not only as inclusions in pyroxenes but also as large chromite crystals (~100 μm in size) in contact with silicates (i.e., plagioclase [Pl] and pyroxene [Cpx, Opx]). b) A few plagioclases, zircon (Zrn), and chromite (Chr) are enclosed by the irregular ilmenite (Ilm) grains; irregular-shaped pockets of silica (SiO_2) and troilite (FeS) attributed to a metasomatic event. c) Abundant presence of merrillite (Mer) with anhedral morphologies (up to 30 μm in size) in fine-grained lithology. d) A shock melt vein (MV) that cut across the coarse and fine lithologies. Note the presence of the sulfur globules (pointed by arrows).

rare earth elements (REE) is identical between the two portions (Table S3), with a flat pattern at ~20 × CI and with a marked negative Eu anomaly (Eu/Eu* = 0.65; Fig. 4). Like REE, most elemental abundances are within ±10% relative between CG and FG portions of Malotas (b), further confirming its monomict nature.

Chemical Compositions of Mineral Phases

Major and minor element compositions in the CG and FG lithologies are given in Tables S1 and S2, respectively. Electron microprobe analyses yielded average compositions of the low-Ca pyroxene that exhibit a homogeneous composition ($Fs_{62.5\pm0.8}Wo_{2.23\pm0.9}$). In the CG portion, the large high-Ca pyroxene grains contain identical chemical compound when compared to exsolution lamellae in the FG portion with $Fs_{26.9\pm0.9}Wo_{43.9\pm1}$. The composition of plagioclase in the CG and FG areas is in average An_{75}, whereas those secondary plagioclases in veinlets are extremely Na-poor ($An_{96.1}$). The silica polymorph present in the eucrite is composed of ~98 wt% SiO_2 with some trace amounts of Fe, Al, Ti, Cr, and Mn (Tables S1 and S2).

The most abundant oxide mineral in both lithologies is chrome spinel. The single crystal chromites in the CG area have higher Al_2O_3 (9.5 wt%) and MgO (0.53 wt%) contents as compared to those of the FG portion (Al_2O_3: 7.5 wt%; MgO: 0.38 wt%), while TiO_2 and FeO show an inverse behavior (2.55 versus 3.1 wt% and 33.5 versus 34.4 wt%, respectively). Chromites intergrown with ilmenite show similar chemical

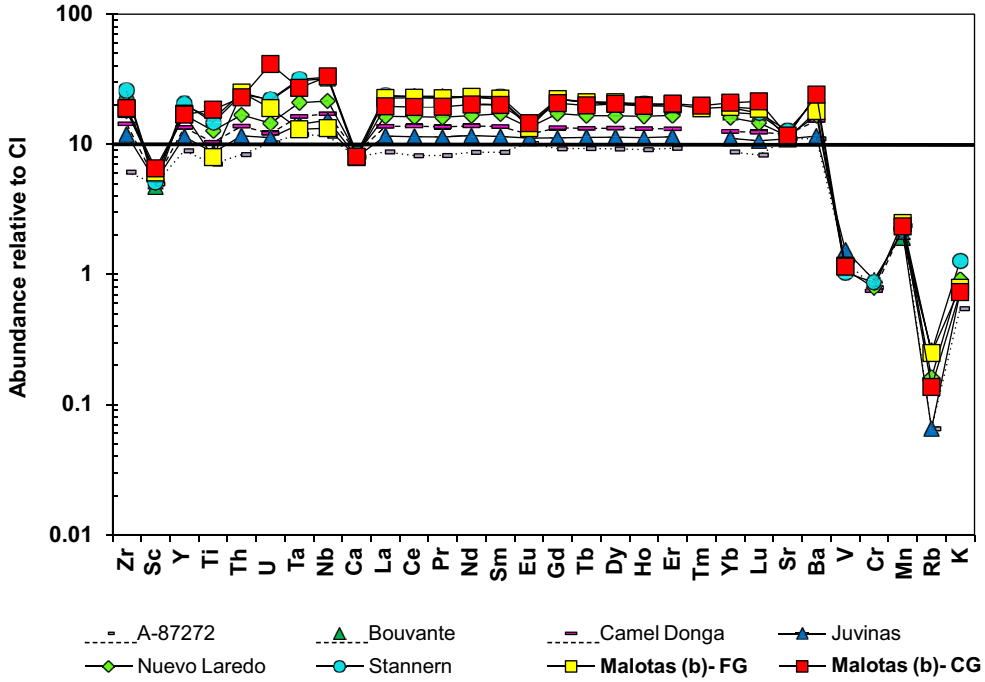

Fig. 4. CI-normalized trace element abundances of coarse-(CG) and fine-(FG) grained lithologies of Malotas (b). Eucrite bulk rock data from Mittlefehldt (2015) are given for comparison. Data are presented relative to Cl chondrite values from Lodders and Fegley (1998). (Color figure can be viewed at wileyonlinelibrary.com.)

compositions as single crystal chromite. The chemical composition of ilmenites in the CG and FG portions is similar (Tables S1 and S2). F-apatite and merrillite grains display low totals (Tables S1 and S2) in the range of ~95 wt% in both lithologies, which is mainly attributed to the typical incorporation of a few wt% of Y, REE, and the actinides U and Th into the crystal structure (e.g., Ward et al., 2017), elements which are not measured here. The chemical compositions in apatites are rather constant, for both portions. Variations have been detected only in the FeO content (0.68 versus 0.43 wt%; Tables S1 and S2).

Geothermometry

For estimating closure temperature of Malotas (b), we used the QUILF (quartz–ulvospinel–ilmenite–fayalite) two-pyroxene geothermometer (Andersen et al., 1993). The data values for augite–orthopyroxene pairs in the FG and CG areas, as well as the equilibration temperatures obtained, are summarized in Table S4. The equilibration temperatures obtained for pyroxene are 726–805 °C and 700–732 °C in the FG and CG areas, respectively. The temperatures determined for FG show an uncertainty of 62–91 °C, while those of the temperatures for CG are with 57–69 °C lower (Table S4).

Noble Gases

The Ne isotopic compositions of all samples (H5, L5 ordinary chondrites and the eucrite fragment) are purely cosmogenic (Fig. 5). The $^{3}He/^{4}He$ ratios of ~31×10^{-4} in the H5 chondrite, ~739×10^{-4} in the L5 chondrite, and ~ 52×10^{-4} in the eucrite are, as expected, significantly higher than primordial components, typically lower than 2×10^{-4} (e.g., Busemann et al., 2000; Huss & Lewis, 1994) and air with a $^{3}He/^{4}He$ ratio of 1.38×10^{-6} (Mamyrin et al., 1970). This shows that also He is strongly influenced by cosmogenic He ($^{3}He/^{4}He = 0.16$; Alexeev, 1998) in all samples, most visible in the L5 chondrite with the highest $^{3}He/^{4}He$ ratios (Table S5). Helium-3 is assumed to be fully cosmogenic. Argon is purely cosmogenic in the eucrite ($^{36}Ar/^{38}Ar \sim 0.64$; $^{36}Ar/^{38}Ar_{cos}$ in achondrites = 0.63–0.65; Wieler, 2002). The two ordinary chondrites have higher $^{36}Ar/^{38}Ar$ ratios (H5 4.15–4.51; L5 0.95–2.71), that is, they contain some trapped Ar, either air ($^{36}Ar/^{38}Ar = 5.305$; Lee et al., 2006), Q ($^{36}Ar/^{38}Ar = 5.34$; Busemann et al., 2000), or a mixture of the two. The uncertainties on the isotopic ratios of Kr and Xe are too large to distinguish between different noble gas components (Tables S6 and S7). Due to the lack or Kr data in some samples and the almost pure cosmogenic Ar in the eucrite, we can

only evaluate trapped $^{36}Ar/^{84}Kr$ and $^{84}Kr/^{132}Xe$ ratios in the H5 chondrite. The ratios in this sample ($^{36}Ar_{tr}/^{84}Kr \sim 80$ and $^{84}Kr/^{132}Xe \sim 1.4$) agree with a mixture of the Q component and air.

To determine CRE ages, we need to know the concentrations of cosmogenic nuclides and their production rates. It is known from previous studies that CRE ages based on ^{38}Ar tend to scatter more than those based on ^{3}He and ^{21}Ne due to heterogeneous target element distribution (e.g., Di Gregorio et al., 2019). We consider the ^{21}Ne ages most reliable as they are less affected by gas loss than the ^{3}He ages and less affected by sample heterogeneity than the ^{38}Ar ages. The ranges in ages are the result of uncertainty on the measured concentrations of noble gases and of the uncertainty on $(^{22}Ne/^{21}Ne)_{cos}$ ratios in the samples, as this shielding indicator influences the production rates produced by the models. For the Malotas (b) eucrite and the Malotas H5 ordinary chondrite, this variation in $^{22}Ne/^{21}Ne$ was insignificant. Two aliquots of each sample were analyzed and give similar CRE ages for all samples.

The large blank correction on Ar in the ordinary chondrites results in additional uncertainty and we therefore refrained from calculating CRE ages based on ^{38}Ar for the ordinary chondrites. The blank correction was smaller on Ar in the eucrite and the $^{36}Ar/^{38}Ar$ ratio is cosmogenic (Table S8). We therefore determined a CRE age also based on cosmogenic ^{38}Ar ($^{38}Ar_{cos}$) for the eucrite. We used the model by Eugster and Michel (1995) to calculate production rates for the eucrite and the model by Eugster (1988) to determine production rates for the ordinary chondrites. The model by Eugster and Michel (1995) requires elemental compositions of the sample as input data; we used the values in Table S3. The production rates are given in Table S9.

The three samples have different CRE ages (Fig. 6). Based on $^{21}Ne_{cos}$, the H5 chondrite has the lowest CRE age of 3 Ma, the L5 chondrite the highest age of 45–52 Ma, and the eucrite an intermediate age of 27 Ma (Table S9). As commonly observed in meteorites, the ^{3}He ages are slightly lower than the ^{21}Ne ages for the eucrite at 21–22 Ma, presumably due to gas loss. Plagioclase, a major mineral in eucrites, is less retentive to noble gases than some other rock-forming minerals and noble gases hosted in plagioclase might therefore have suffered from diffusive losses (Herzog & Caffee, 2014). This could affect both He and Ne (Herzog & Caffee, 2014). We nevertheless discuss the Malotas (b) eucrite CRE age based on Ne in the following as CRE ages based on Ar often are affected by heterogeneous distribution of target elements. Slight gas loss could also have lowered the ^{3}He CRE age of the H-chondrite to 2 Ma.

We estimated the ^{40}Ar retention ages of the samples based on the measured concentrations of ^{40}Ar (Table S10) and K (Table S3) for the eucrite and literature values of K for the two chondrites (Wasson & Kallemeyn, 1988). Based on the measured concentrations of ^{40}Ar (Table S10) and K (Table S3), it is not possible to distinguish between Ar-air and Ar-Q. Argon in air has a $^{40}Ar/^{36}Ar$ ratio of ~298.6 (Lee et al., 2006) while Q is essentially void of ^{40}Ar

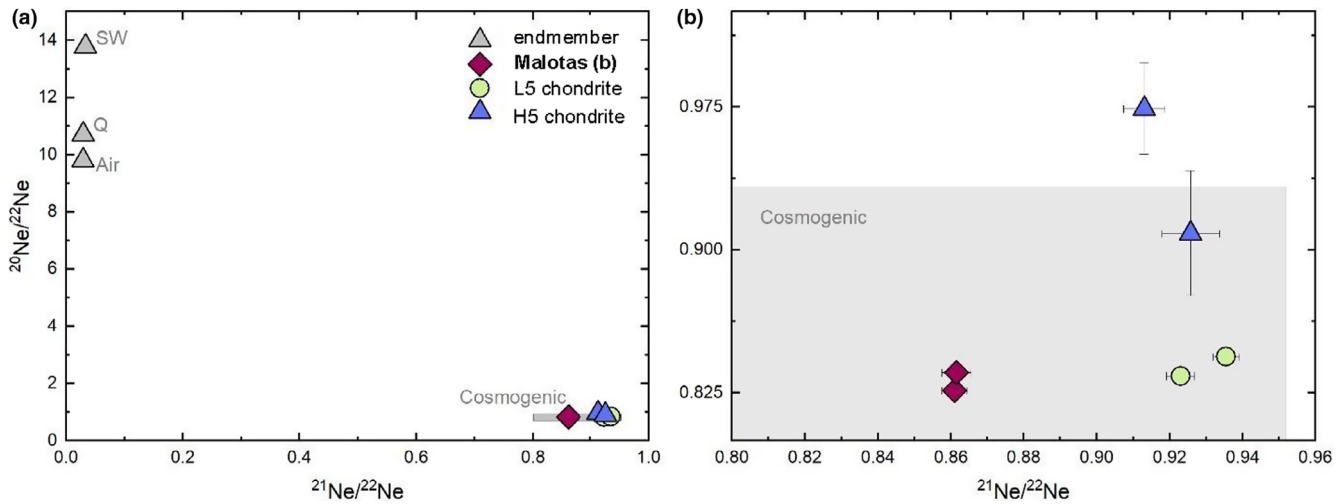

Fig. 5. Ne isotope composition of the samples. Panel b is zoomed into the area of cosmogenic Ne where the sample data points plot (a). All samples have essentially pure cosmogenic Ne. The lower cosmogenic $^{21}Ne/^{22}Ne$ ratios for eucrite Malotas (b) could reflect the lower Mg content in eucrites compared to that in ordinary chondrites (~5 wt% versus ~14 wt%, respectively, e.g., Lodders & Fegley, 1998) or different shielding conditions of the samples in the meteoroid(s). The gray field in (b) shows typical cosmogenic Ne compositions (Wieler, 2002). (Color figure can be viewed at wileyonlinelibrary.com.)

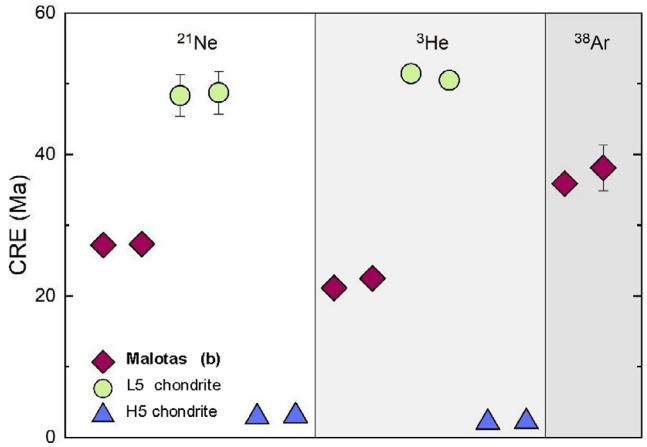

Fig. 6. Calculated CRE ages for the H5 (Malotas) and L5 ordinary chondrite and the Malotas (b) eucrite, which are clearly distinct. The ^{3}He ages determined for the eucrite and the H5 chondrite are slightly lower than those determined based on ^{21}Ne suggesting some heat-induced loss of ^{3}He. CRE ages based on ^{38}Ar were only determined for the eucrite and are higher than the ^{3}He and ^{21}Ne ages, possibly due to target element heterogeneity. We consider the ^{21}Ne ages to be most reliable. For the eucrite, the model by Eugster and Michel (1995) was used to determine production rates, and for the two ordinary chondrites, the model by Eugster (1988) was used. (Color figure can be viewed at wileyonlinelibrary.com.)

(Busemann et al., 2000). We therefore calculated ^{40}Ar retention ages for the two ordinary chondrites assuming both (i) all trapped Ar to be Q and therefore all ^{40}Ar to be radiogenic and (ii) assuming all trapped Ar to be air, and corrected the concentration of ^{40}Ar accordingly (Table S10). The ^{40}Ar ages scatter around 4 Ga for all samples. The ages assuming the trapped Ar to be air are naturally slightly lower than the ages assuming all trapped Ar to be Q; however, this does not change the general picture that all samples have similar ^{40}Ar retention ages.

The (U-Th)/He ages were estimated based on ^{4}He concentrations corrected for cosmogenic He assuming $(^{3}He/^{4}He)_{cos} = 0.16$ (Alexeev, 1998), measured concentrations of Th and U in the eucrite (Table S3), and literature values for U and Th in the ordinary chondrites (Wasson & Kallemeyn, 1988). The He retention ages differ between the three samples, ~1.2 Ga for the eucrite, ~1.9 Ga for the L5 chondrite, and ~3.2 Ga for the H5 chondrite (Table S10).

Scatter between the different aliquots of the H5 and L5 ordinary chondrites indicates that the samples either experienced heterogeneous He-loss or have heterogeneous chemistry, making the ages uncertain. In the L chondrite, suggested He loss must have occurred before or during the ejection from the parent body as there is no evidence for loss of He in the CRE ages (Table S9). In the H chondrite, He loss could potentially partially also have occurred during transit to Earth as the ^{3}He CRE ages are lower than the ^{21}Ne ages. The two aliquots of the eucrite have similar ^{4}He concentrations and hence similar (U-Th)/He ages.

Oxygen Isotopic Composition

Replicate analyses of oxygen isotopes (‰), obtained by the laser fluorination method yielded values of: $\delta^{17}O^{*}$ of 1.785 and 1.775; $\delta^{18}O$ of 3.779 ± 0.003 and 3.787 ± 0.005; $\Delta^{17}O$ of −0.208 ± 0.006 and −0.222 ± 0.007. The results of this study jointly with all major HED rock types are shown in Fig. 7.

DISCUSSION

From a chemical point of view, eucrites are broadly divided into two subtypes: (1) cumulate eucrites, which are medium-grained to CG gabbros, and (2) basaltic eucrites (noncumulate), which are FG to medium-grained basalts (<2 mm grain sizes; e.g., McSween et al., 2011, Mittlefehldt, 2015; Takeda, 1991). Variations in their bulk chemical composition allows classifying them into four distinctive chemical subgroups: Main Group, Stannern-trend, Nuevo Laredo-trend, and residual eucrites (Mittlefehldt et al., 1998; Stolper, 1977; Warren & Jerde, 1987; Yamaguchi et al., 2009). These subgroups are differentiated based on their Mg# (=100 × molar Mg/[Fe+Mg]), Ti content, and incompatible trace element abundances. In addition, Main Group and Nuevo Laredo-trend eucrites display wide variations in their Mg# with moderate variations in incompatible element abundances (e.g., Stolper, 1977; Warren & Jerde, 1987). The residual and Stannern-trend eucrites share similar major element abundances with the Main Group eucrites but are characterized by distinctive trace element abundances. The former show light REE depletions and positive Eu anomalies (Yamaguchi et al., 2009), while the latter are significantly richer in Ti and in incompatible trace elements characterized by a significant negative Eu, Sr, and Be anomalies (Barrat et al., 2007; Mittlefehldt, 2015; Schiller et al., 2010; Stolper, 1977). Considering only La and Sc trace elements abundances, Mittlefehldt and Lindstrom (1993) proposed that a clear discrimination can be made among the basaltic eucrites: the Stannern trend with high La and moderate Sc; the Main Group with low to moderate La and Sc, and the Nuevo Laredo-trend eucrites with moderate La and high Sc.

The vast majority of eucrites experienced a complex postcrystallization history, including a prolonged thermal metamorphism and brecciation. Takeda and Graham (1991) studied the homogenization of eucritic

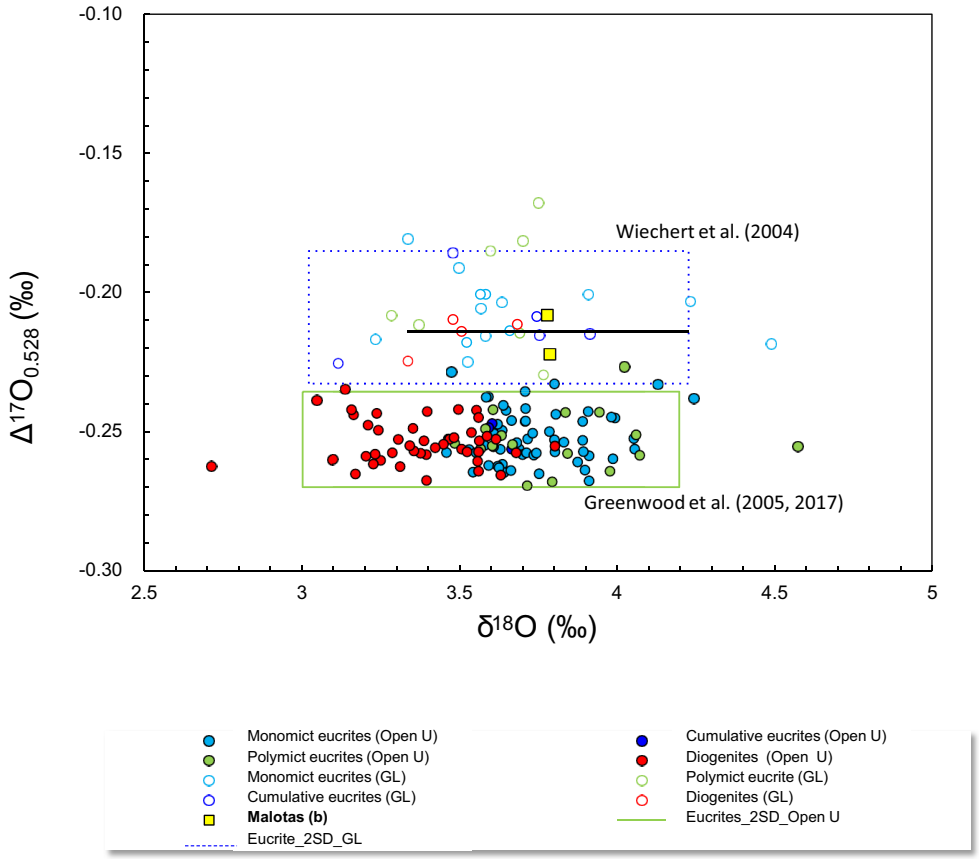

Fig. 7. Oxygen isotope variation diagram showing mean values of $\Delta^{17}O$ versus $\delta^{18}O$ for Malotas (b) compared with HEDs. $\Delta^{17}O$ value from this study is very close to that of eucrite fractionation line (EFL) with a mean $\Delta^{17}O$ value of -0.239 ± 0.007 (Greenwood et al., 2005). (Color figure can be viewed at wileyonlinelibrary.com.)

pyroxenes as a guide to define their thermal history. They divided eucrites into six types (type 1–6), reflecting increasing degrees of thermal metamorphism. An additional type 7 has been later added by Yamaguchi et al. (1996) considering that most eucrites could have undergone at least one subsolidus reheating event resulting from impact or lava flows extruded over a primary lava.

Below, we discuss the petrographic features, chemical composition (major, minor, and trace element abundances), and the oxygen isotopes data in order to classify Malotas (b). In addition, the CRE ages both from Malotas (b) and from the related ordinary chondrites found at the same site are given in order to definitively clarify the Malotas 1931 fall.

Origin and Genetic Relationship

The $\Delta^{17}O$ of Malotas (b) is within the range of the published Eucrites–Diogenites data of Wiechert et al. (2004) but higher than the 2SD range of Eucrite–Diogenite of Greenwood et al. (2005, 2017). Greenwood et al. (2005) inferred that the discrepancy of $\Delta^{17}O$ values between the laboratories may reflect calibration differences and/or potential terrestrial contamination for the data of Wiechert et al. (2004). However, even for the HED falls, the data reported by Wiechert et al. (2004) are higher than the data of Greenwood et al. (2005). Malotas (b) is very fresh and the analyzed sample was pretreated using the same method as applied by Greenwood et al. (2005). Thus, it is unlikely that the higher $\Delta^{17}O$ value of Malotas (b) was modified by terrestrial contamination. The oxygen isotope data suggest that Malotas (b) is a basaltic eucrite.

Petrology and Chemical Composition

Characterization of most areas of the investigated eucrite sections revealed a simple petrography, in which original igneous textures are preserved. Malotas (b)

is composed of basaltic material with chemical compositions nearly identical among several lithic clasts and matrix regions (Tables S1 and S2; Fig. 2). The texture of Malotas (b), both macroscopically and microscopically, indicates that it was mechanically mixed on the parent body's surface into a breccia. The CG lithology is characterized by a subophitic to ophitic texture, similar to other monomict eucrites (e.g., Duke & Silver, 1967; Mittlefehldt et al., 1998). In the FG lithology, occurrence of several areas characterized by recrystallized pyroxene and plagioclase grains of ≤10 μm with 120° triple junctions indicates an intense metamorphic event after crystallization of rock-forming silicates (Fig. 2f; Fig. S1 in supporting information). Such recrystallized pockets were also found in some other HEDs, such as the Puerto Lápice main group basaltic eucrite (Llorca et al., 2009). The pyroxene grains in each lithology show homogeneous Mg-Fe composition. However, they are inhomogeneous in their Fe-Ca contents due to exsolution of augite from host pigeonite, a common feature in equilibrated eucrites (e.g., Reid & Barnard, 1979). Based on the metamorphic classification scheme of Takeda and Graham (1991), Malotas (b) corresponds to a petrologic type 4. This is consistent with homogeneous host pyroxene and remnant of zoning, recrystallized and exsolution of augite resolvable by EMPA (Figs. 2 and 3), which are typical features of basaltic eucrites and further inferred from Cr-spinel chemistry (Yamaguchi, 2000).

Bulk Chemical Composition

The bulk chemical compositions have been used to classify and to understand the nature of melting processes of the precursor eucrites (e.g., Stolper, 1977). The Mg# of 38 in the FG and CG portions of Malotas (b) is similar to those of most Main Group eucrites (e.g., Juvinas, Mg# 40; Duke & Silver, 1967; McCarthy et al., 1973) and significantly lower than those of cumulate eucrites (e.g., Moore County, Mg# 50; Hess & Henderson, 1949; McCarthy et al., 1973). The abundances of Co, Ni, Ti, and Cu are higher in the CG portion relative to the FG lithology by a factor of about 2 (Table S3). In Fig. 2c, abundant F-apatite and the presence of ilmenite and chromite filling the fractures in the rims of large orthopyroxene (Opx, 500 μm in apparent size) in the CG lithology should be noted. Consistent with this observation, the disparity in TiO_2 and especially in Ti/REE, is not related to the grain size but to the fact that Opx rims are more abundant in the CG lithology, and therefore, the Ti and P are more abundant. Thus, in addition to Mg and Si, the metasomatic fluid was carrying P, Ti, and Fe (e.g., element mobilization by fluids; Rombeck et al., 2021), although Fe was not sufficiently abundant in the fluid to produce Fe-rich rims in the Opx nor to give rise to fayalitic olivine veins.

The overall REE element pattern for Malotas (b) is within the range of other basaltic eucrites and clearly shows that the sample belongs to the chemical subgroup of Stannern-trend eucrites (e.g., Barrat et al., 2007) (Fig. 4). The eucrite is richer in incompatible elements than most eucrites with about 20 × CI, which is also typical for Stannern-trend eucrites. The enrichment in Th is the same as for La and other REE. The abundances of Ti, Nb, and Ta in the CG portion are higher, due to higher abundances of ilmenite in the rims developed on large Opx grains that carry the P, Ti, and Ca, as seen in Fig. 2c. REE abundances are broadly similar between the two lithologies with light REE about 10% lower in the CG lithology, despite the higher P and U abundances. This implies that REE were not significantly transported by the metasomatic P-Ti-Fe fluid. The Th/U value of the CG portion is lower (2.0 versus 4.8) than that of the FG portion that also corresponds to a difference in the P_2O_5 abundance. Here, Th is in line with REE and many other incompatible elements, while U is enriched by a factor of about two in the CG lithology, similar to P, Ta, Nb, and Ti, because of the presence of fluorapatite (F-Ap) veinlets within pre-existing fractures and crystallographic cleavage planes on large Opx grains (Fig. 2c). Zircon is another major host for heavy REE, so its presence, typically interstitial to silicates, in late-stage melt pockets or exsolved from ilmenite (e.g., Roszjar et al., 2014) could affect the bulk REE concentration of the lithic portion as well. However, Zr and heavy REE abundances are consistent between the FG and CG portions of the section. Ratios like Nb/Ta, Zr/Hf, and La/Th are near chondritic values.

As indicated above, variations between major and trace element abundances and ratios can help to discriminate between the various chemical groups of basaltic eucrites (e.g., Barrat et al., 2000; Kagami et al., 2019; Mittlefehldt, 2015). The diagram of La versus FeO/MgO ratio shows that the CG and FG portions are well resolved inside the area defined for the Stannern trend (Fig. 8), even though the FG portion has higher La abundances than the CG portion (5.33 versus 4.60 wt%). In any case, we should always keep in mind that the availability of a growing database can make the trends among basaltic eucrites more complex (McSween et al., 2011).

Chemical Composition of Mineral Phases

Pyroxene

The Fe/Mn values of pyroxene and the oxygen isotopic compositions of basaltic eucrites have been

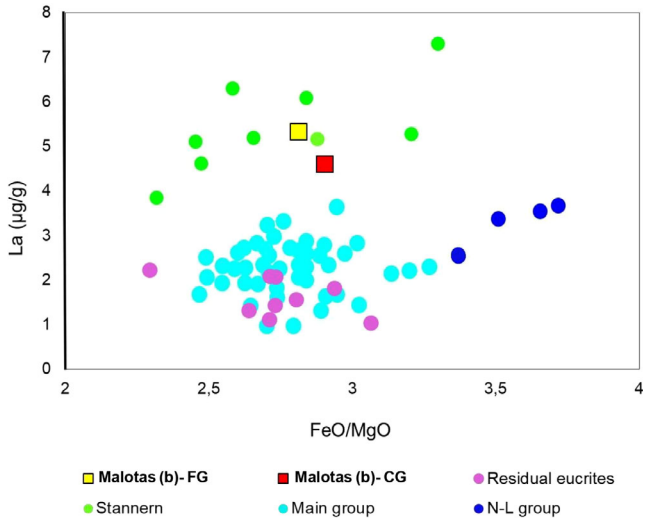

Fig. 8. La versus FeO/MgO plot of coarse-(CG) and fine-(FG) grained portions of Malotas (b) obtained by La-ICP-MS, compared with other basaltic eucrites. Basaltic eucrites are distinguished into four different chemical groups: Main Group, Nuevo Laredo (N–L)- and Stannern trend, and residual eucrites. Malotas (b) belongs to the group Stannern-trend basaltic eucrites. Reference data are taken from Mittlefehldt (2015) and Kagami et al. (2019). (Color figure can be viewed at wileyonlinelibrary.com.)

widely used as a means of evaluating potential genetic links between these meteorites. Comparative planetary mineralogy studies (e.g., Karner et al., 2003; Papike, 1981, 1998; Papike et al., 2003, 2005) show that elemental signatures in minerals from planetary basalts record planetary parent ages and processes that affect basaltic magmatism, like igneous setting and differentiation. Papike (1998) used a suitable method for comparing the variability of Mn (atoms per formula unit = afu) versus Fe (afu) in pyroxenes. The respective Fe/Mn value (32.6 ± 1.7) for Malotas (b) pyroxenes is within uncertainty indistinguishable to the value assigned to 4 Vesta (Fe/Mn = 30 ± 2; Mittlefehldt, 2005; Papike et al., 2003).

F-Apatite

The chemical compositions of F-apatite grains in Malotas (b) resemble those of other eucrites (e.g., Sarafian et al., 2013; Ward et al., 2017). The chemical composition of F-apatite, belonging either to the CG or FG fractions or veinlets inside large high-Ca pyroxenes, falls within the area corresponding to basaltic and cumulate eucrites (Fig. 9). Previous investigations (e.g., Jones et al., 2014; McCubbin et al., 2014; Patiño-Douce & Roden, 2006; Sarafian et al., 2013; Ward et al., 2017; Zhang & Yurimoto, 2013) have studied the presence of apatite in a large collection of planetary materials. These studies allowed differentiating the F-Cl-OH abundances of apatite in the areas of each group of meteorites (e.g., Patiño-Douce & Roden, 2006). For example, eucritic apatites exhibit a wide range of F atomic proportions from ~0.5 to 1 (e.g., Ward et al., 2017) and are almost exclusively F-apatites (Jolliff et al., 2006). All apatite grains in Malotas (b) are variable in their F to OH ratios, with those corresponding to the CG and FG portions showing a more widespread variation in F-apatite (F = 0.81–1) as compared to those occurring in veinlets (F = 0.90–0.95). As demonstrated in this study, Malotas (b) contains apatite grains and veinlet-apatite included in pyroxene and apatite grains associated with ilmenites. This result is similar to that from Sarafian et al. (2013), who attributed this observation to two different events. Those apatite grains included in pyroxenes suggest that this apatite crystallized early. While those apatite grains associated with ilmenites crystallized from a residual melt (F-rich, metasomatic process), and are texturally similar to those observed in most apatites in basaltic eucrites such as Bates Nunataks 00300, Lewis Cliff (LEW) 88009, LEW 88010, EET 87542, EET 90020, Nuevo Laredo, and Stannern as well as the cumulate eucrites Allan Hills 85001 and Serra de Magé (Sarafian et al., 2013). Therefore, all apatite grains fall within the expected F atomic range of basaltic eucrites, as defined by Ward et al. (2017).

Spinel

Cr-spinel is a common minor mineral (≤0.5 vol%) in basaltic eucrites (Mittlefehldt, 2015; Yamaguchi, 2000). The chromite grains provide evidence of the meteorites' thermal history. The chemical composition of all studied chromite grains points toward this mineral being affected by thermal metamorphism, belonging to type 4 according to Yamaguchi (2000) (Fig. 10). Slight variations in the endmember compositions were detected from Cr-spinel grains of CG and FG portions ($Chr_{69.3}$ versus $Chr_{71.7}$, respectively). In addition, the FG area exhibits significantly higher TiO_2 contents (2.5–6.5 wt%, Tables S1 and S2). Conversely, chromite intergrowths with ilmenite in both CG and FG portions show similar chemical composition (Fig. 9).

Thermal and Metasomatic Events

The estimated closure temperatures for Malotas (b) ranging between 700 and 805 °C with uncertainties of 60–91 °C (Table S4) indicate that the chemical compositions of the mineral phases have not reached a perfect equilibrium as indicated by models (Andersen et al., 1993). However, these estimated temperatures for Malotas (b) are very reasonable for the last stages of exsolution and agree with the

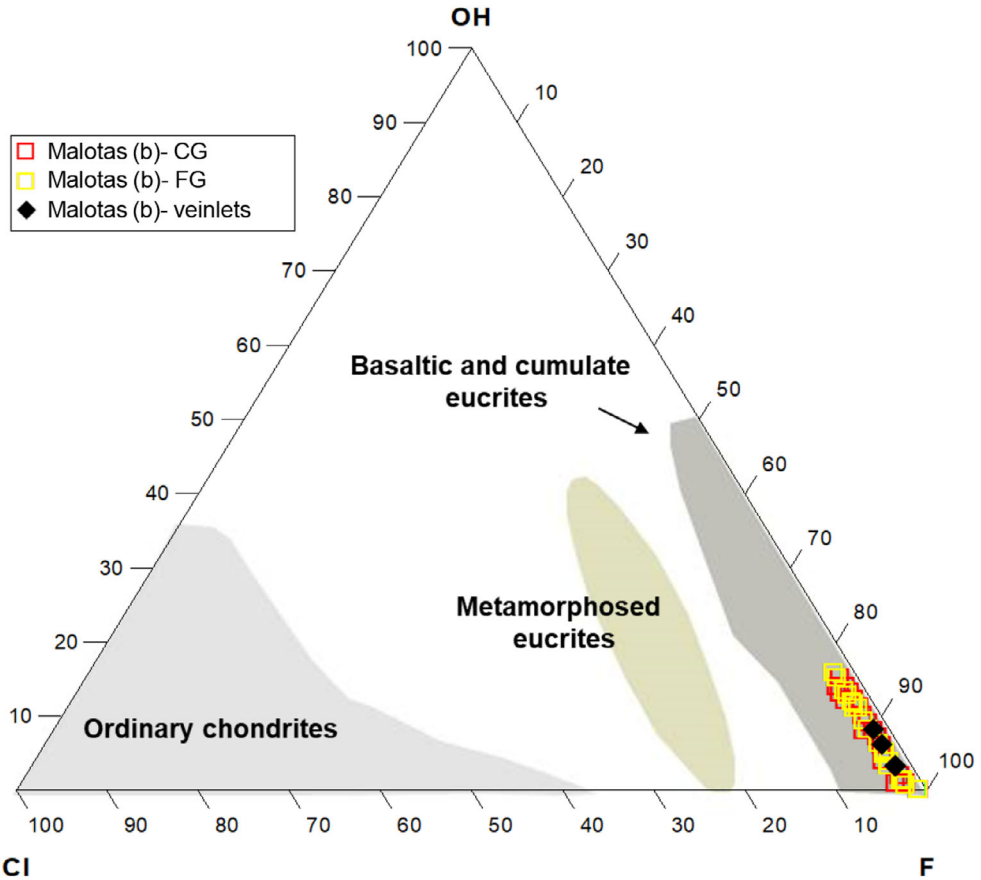

Fig. 9. Ternary plot of the volatile (F, Cl, OH-) compositions (atomic proportions) of apatite grains in Malotas (b) relative to some other meteorite groups. Rhombus and open squares correspond to individual analyses from this study, while the shaded areas illustrate the ranges of data published by Patiño-Douce and Roden (2006), Sarafian et al. (2013), Zhang and Yurimoto (2013), Jones et al. (2014), McCubbin et al. (2014), and Ward et al. (2017). (Color figure can be viewed at wileyonlinelibrary.com.)

equilibration temperatures for basaltic eucrites from 730 to 980 °C reported in the literature (e.g., Yamaguchi et al., 1996). The metamorphic events affecting the basaltic, type 4 eucrites (e.g., Stannern, Bouvante, Nuevo Laredo) have acquired temperatures of metamorphic equilibration at ~800 °C (Barrat et al., 2007) while the polymict eucrites Northwest Africa (NWA) 6105 and NWA 6106 reached them within a temperature range of 652–886 °C (Singerling et al., 2013). The lower temperatures (i.e., ≤730 °C) observed in the literature are akin to those obtained mainly in the CG lithology for Malotas (b) (Table S4) and may indicate that some clasts could have experienced extremely slow cooling consistent with results from Singerling et al. (2013). If comparison is extended to other members of the HED clan (e.g., diogenites), the estimated closer temperatures of Malotas (b) are in good agreement to those calculated by applying similar two-pyroxene methods for diogenites (650–880 °C; Mittlefehldt, 1994).

The textural relationship between ilmenite and zircon is another indicator of the thermal history. Numerous studies on eucrite zircon grains indicate that they can be formed (i) during a global metamorphic event that occurred at a very early stage on the eucrite parent body (Haba et al., 2014; Iizuka et al., 2015; Liao & Hsu, 2017) or (ii) they can be crystallized under igneous conditions as proposed previously for the least-metamorphosed samples (e.g., Misawa et al., 2005; Roszjar et al., 2016; Zhou et al., 2013). Haba et al. (2014) indicated that the maximum sizes of zircon grains in eucrites seem to be related to the metamorphic grade and be the result of crystallization and/or overgrowth during partial melting of the mesostasis region. The Malotas (b) sample contains large zircon grains with a maximum size of ~25 μm, similar to those observed for highly metamorphosed eucrites (Yamato [Y] 792510 and Asuka [A] 881467; Haba et al., 2014). In Malotas (b), exsolution of zircon from ilmenite possibly took place during a subsolidus reheating event.

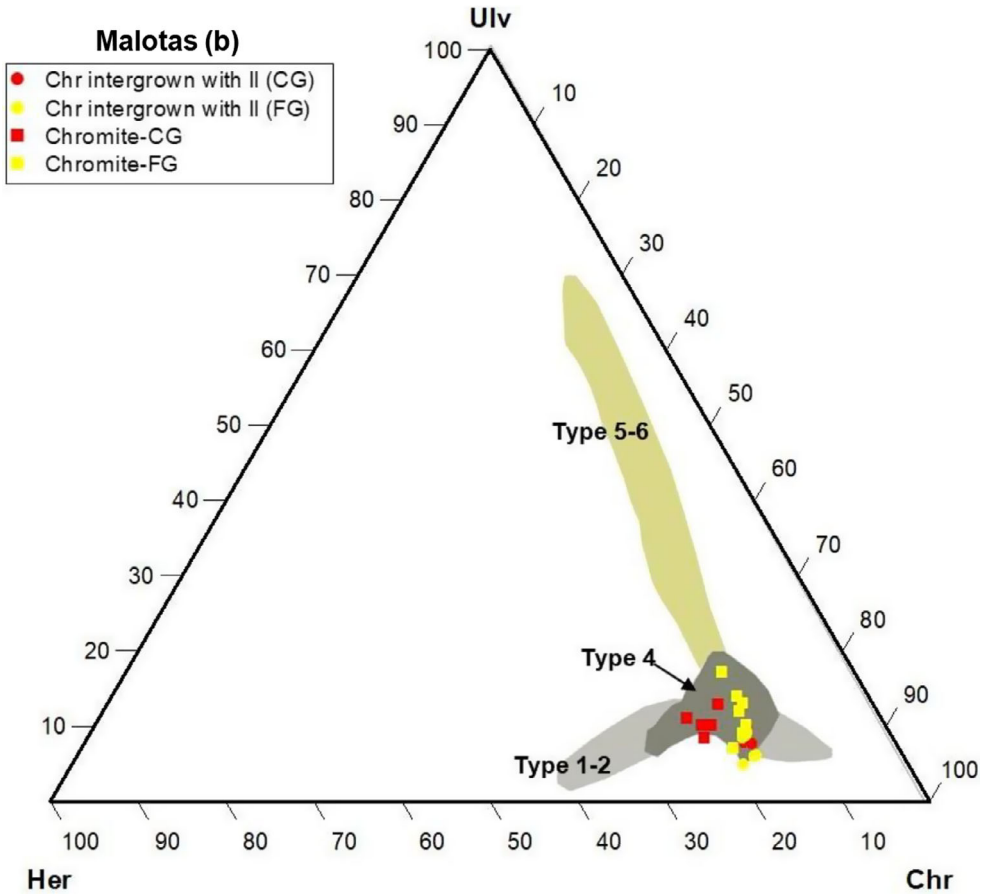

Fig. 10. Ternary plot of chemical compositions of spinels in eucrites. Colored fields mark the ranges of metamorphism obtained by Yamaguchi (2000) and Mittlefehldt (2015). The squares and circles correspond to analyses of large chromite grains in the silicate matrix of Malotas (b) and chromite grains intergrown with ilmenite of (a) coarse- and (b) fine-grained portions. Her = hercynite; Ulv = ulvöspinel; Chr = chromite. (Color figure can be viewed at wileyonlinelibrary.com.)

However, these results cannot be generalized to other eucrites (e.g., unmetamorphosed eucrites) as the occurrence of large zircon crystals (i.e., ≥30 μm) was also described in the unmetamorphosed, basaltic eucrite NWA 5073 (Roszjar et al., 2011).

Metasomatism

Only few basaltic eucrites and eucrite clasts in howardites have been discussed to be affected by metasomatic events and most exhibit metasomatic alteration features typically occurring on a small scale. Several features that are attributed to these metasomatic reactions include: Fe-enrichments of pyroxenes along cracks (Barrat et al., 2011); fayalitic veins that cross pyroxene grains (Barrat et al., 2011; Roszjar et al., 2011), which are also found in the recently observed basaltic eucrite fall Serra Pelada (Zucolotto et al., 2018); secondary Na-poor plagioclase (Barrat et al., 2011; Warren et al., 2014); microveins dominated by other phases such as Cr-spinel and silica with traces of ilmenite, troilite, and probably also zircon (e.g., NWA 5738; Warren et al., 2014); the breakdown of pyroxene to silica and troilite (Mayne et al., 2016; Pang et al., 2017; Zhang et al., 2013), among others. The majority of these features are included in the different alteration models proposed by Barrat et al. (2011).

In Malotas (b), only three of the abovementioned features have been identified: (1) secondary veinlets mainly composed of anorthitic plagioclases and veinlet apatite that cross high-Ca pyroxene grains; (2) chromite, troilite, and ilmenite-in-pyroxene inclusions (Fig. 2c); and (3) highly porous SiO_2 polymorphs (Fig. 11), and irregular-shaped pockets of silica and troilite (Fig. 3b). The latter might be the product of the breakdown of pyroxene and was initially considered evidence of secondary chemical alteration (Duke & Silver, 1967) but later attributed to a metasomatic event (Barrat et al., 2011).

The lack of fayalitic veinlet makes Malotas (b) unique among eucrites with extensive metasomatism

(Warren et al., 2014). The host pyroxene could have acted as a major host for Mg and Fe first and, therefore, the system could get oversaturated in Si, Ca, Al, and other available elements leading to the formation of Pl veins and silica polymorphs but insufficient to form fayalitic olivine. The lack of Fe-enrichment in Opx rims as well as of fayalitic olivine veins inside the fractures of pyroxene may point toward the absence of aqueous fluids that could have served as metasomatic media regardless of whether the fluid contained Fe or not, as shown by the experimental work of Rombeck et al. (2021).

The compositions of plagioclase grains ($An_{96.1}$) associated with the veinlets are more calcic than those of primary plagioclase ($An_{77.6}$). The Na-rich composition of the plagioclase (average $An_{77.6}$) is uncommonly sodic for a eucrite. However, this composition is the second most-albitic plagioclase composition reported to date for eucrites with only NWA 5738 (An_{74}; Warren et al., 2014) being lower and falling in the range of the lower values shown by Mayne et al. (2009). Also, F-apatite grains in veinlets are more enriched in FeO (1.84 wt%) as compared to those in the CG and FG lithologies (Tables S1 and S2). F-Apatite was also found in fayalitic olivine veins or apatite–merrillite replacement in, for example, Juvinas, NWA 5073, or Serra Pelada (e.g., Roszjar, 2019; Roszjar et al., 2011; Sarafian et al., 2013).

Although all the previously mentioned features have been attributed to a metasomatic event, the mechanism that causes this secondary chemical alteration is a matter of debate. Fluid-driven alteration (Barrat et al., 2011; Chen et al., 2015; Warren et al., 2014) and vapor-driven alteration (Schwartz & McCallum, 2005; Zhang et al., 2013) are the two most discussed processes. Alternatively, a high-temperature process such as incongruent melting in situ of primary pyroxene could be a possible process to generate Fe-rich olivine and anorthitic plagioclase in cracks and interstices (Patzer & McSween, 2018; Roszjar et al., 2011). However, more recent studies (e.g., Pang et al., 2017; Vollmer et al., 2020) showed that the incongruent melting model cannot account for the occurrence of the Fe-rich features along cracks crosscutting both nonequilibrated and equilibrated pyroxenes. Therefore, the occurrence of Fe-rich veins in unmetamorphosed pyroxenes (e.g., Vollmer et al., 2020) supports a late-stage metasomatism scenario, probably caused by a degassing magma ocean (Sarafian et al., 2017). Recently, Rombeck et al. (2021) performed a series of heating and hydrothermal experiments with liquids of different Fe-enriched compositions. These led them to conclude that the metasomatic reactions of aqueous liquids with basaltic eucrite minerals could explain the presence of veinlet-like textures with Fe-enrichments and/or fayalitic olivine grains inside the fractures of pyroxene. However, they do not discount that some of these features could be the result of a high-temperature process.

Clear evidence of fluid–rock interactions as those displayed in the Serra de Magé cumulate eucrite (Treiman et al., 2004) as well as the presence of Fe-rich phases as those observed in almost every experiment of Rombeck et al. (2021) are, however, absent in Malotas (b), making a pure liquid-driven metasomatic event unlikely. The breakdown of pyroxene to troilite and silica could involve the presence of a sulfur vapor (e.g., S-O-P vapor) as proposed by Zhang et al. (2013). Such phase could also be responsible for the chemical change of plagioclase in secondary veinlets through

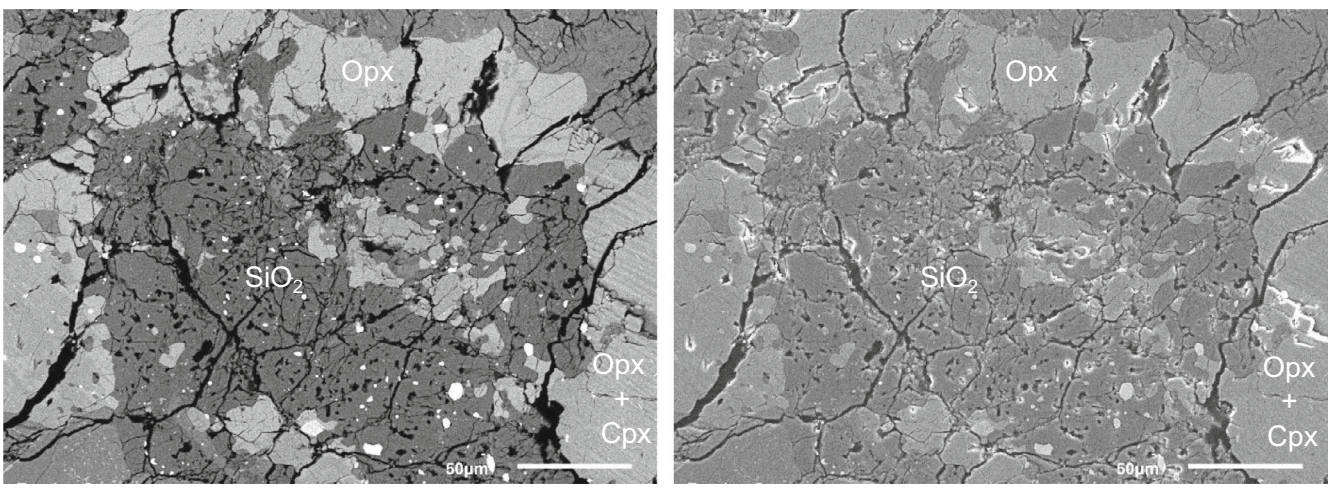

Fig. 11. SEM images (left, BSE; right, secondary electron [SE]) of the silica polymorph–troilite pockets. The SE image allows to see the highly porous nature of silica.

a dissolution/redeposition process from primary plagioclase and apatite (Barrat et al., 2011). The highly porous nature of silica in the silica–troilite pockets (Fig. 11) could point to a vapor-driven alteration, in agreement with some previous studies (e.g., Rombeck et al., 2021).

A Late Thermal Event

Most of the basaltic eucrites have experienced a significant recrystallization that took place during the metamorphic events (e.g., Metzler et al., 1995; Takeda & Graham, 1991; Yamaguchi et al., 1996). The existence of a thermal annealing process affecting Malotas (b) is inferred by the presence of recrystallized pockets, characterized by granoblastic textures of pyroxenes and plagioclases (Fig. 2f). The fact that plagioclases in some of these recrystallized lithic clasts are more calcic ($An_{94\pm0.9}$, $n = 13$) when compared to plagioclase in the silicate matrix (An_{78}; Table S1) while pyroxene grains keep similar chemical compositions, indicate that the recrystallization event induced chemical changes in which Ca enrichment seems to be the one that has prevailed (see Fig. S1).

A last thermal event took place in Malotas (b) after brecciation as evidenced by the presence of a melt vein cross-cutting both lithologies (see Fig. S1). The fact that only one of the studied samples exhibits a single, relatively thin melt vein points to a mild late shock metamorphic event (Barrat et al., 2003; Metzler et al., 1995; Mittlefehldt et al., 2013) that could be attributed to an extensive reworking by impact event(s) on the surface of the parent body. Such a late thermal event is consistent with the variations found in the nominal gas retention ages as determined in this work on six Malotas samples (Table S10). While the U/Th-^{4}He ages are in the range 1.2–3.4 Ga, and scatter widely, which is consistent with late-stage partial resetting, the typically more retentive K-Ar system shows old ages in the range 3.5–4.2 Ga.

Linkage of Malotas (b) to the H5 and L5 Ordinary Chondrites and Ejection of Vestan Material

The cosmic ray irradiation history of Malotas (b) (eucrite), Malotas (H5), and Malotas (c) (L5) can shed some light on whether the samples come from the same meteoroid or if their association is potentially the consequence of a curation mistake that occurred sometime between the Malotas fall of 1931 and the current time. CRE ages date how long a given meteorite sample was located within the top few meters of a meteoroid. In most cases, this corresponds to the time from ejection of the meteoroid from its asteroidal parent body until it fell on Earth, where it is shielded from cosmic rays by the atmosphere. At first glance, the different CRE ages of 3, ~50, and 27 Ma determined for Malotas, Malotas (c), and Malotas (b), respectively, appear to prove that the samples come from different meteoroids. However, impact gardening of asteroidal regoliths leads to an efficient mixing that can result in variable CRE of rocks that are contained in the same meteoroid (e.g., Welten et al., 2011). This was suggested, for example, for the Fayetteville H4 chondrite (Wieler et al., 1989) and the Almahata Sitta polymict anomalous ureilite (Goodrich et al., 2019; Riebe et al., 2017). The latter includes lithologies of different chemical classification including ureilite, CI chondrite-like, enstatite, and ordinary chondrite fragments, which do show distinct exposure ages, similar to the different CRE ages of the lithologies here. Another recent fall which contained different lithologies is the meteorite Motopi Pan, which was observed as asteroid 2008 LA before its impact with the Earth (Jenniskens et al., 2021). Motopi Pan is especially interesting here as it is a HED polymict breccia containing howardite, cumulate, and basaltic eucrite, and diogenite lithologies (Jenniskens et al., 2021). However, in contrast to the Malotas stones, and some of the Almahata Sitta stones, the various lithologies of Motopi Pan have the same CRE age of ~19 Ma (Jenniskens et al., 2021). This differs from the three CRE ages for the Malotas stones obtained in this work (~3, 27, 50 Ma, respectively), and with the current data, there is no clear further relationship between Motopi Pan and Malotas.

The main mass of Malotas, that is, the H5 chondrite, has been studied for its noble gases and irradiation history previously. In contrast to our findings—no solar wind detection in any of the three Malotas lithologies, previous studies found that some fragments of H5 Malotas are gas-rich and have high concentrations of trapped ^{4}He, ^{3}He, and appreciable amounts of Ne implanted by the solar wind (e.g., Srinivasan, 1977). Such solar wind gases are only implanted into the top nanometers of grain surfaces and are therefore generally seen as evidence that the sample is a regolith breccia. The lack of solar wind in the Malotas (H5) sample studied here (and by Zähringer, 1966), which also holds for the Malotas L5 and eucrite samples, shows that solar wind implantation must have been heterogeneous on the Malotas parent body. The L5 and eucrite lithologies may originate from deeper layers in their original parent bodies and where also protected from exposure to solar wind on the secondary Malotas (H) parent body. Srinivasan (1977) detected discrepancies between ^{26}Al activity and ^{21}Ne CRE ages in Malotas, with exposure ages of 1.1×10^6 year and 2.8×10^6 year, respectively. Cressy and Bogard (1976) obtained a similar discrepancy:

lower ^{26}Al CRE ages compared to ^{21}Ne CRE ages. These observations indicate that the Malotas H5 chondrite may have been pre-irradiated in an asteroidal regolith (e.g., Srinivasan, 1977; Wieler et al., 1989), similar to pre-irradiated xenoliths found in the gas-rich Weston H4 ordinary chondrite (Schultz et al., 1972).

Therefore, we cannot rule out that all three lithologies may have originated from the 1931 meteorite fall. For example, if the H5 chondrite fraction originated from the H parent body's surface, impact gardening could have resulted in an efficient mixing so that other material impacting the surface (e.g., eucritic and L5 chondritic material) was incorporated into the main H5 mass with variable CRE ages. Consequently, all the three Malotas samples (H5, L5, and eucrite) could be samples derived from the breakup of a polymict meteoroid or even asteroidal parent body, 3 Ma ago, lining up with other more recent discoveries such as the Almahata Sitta polymict anomalous ureilite connected to the 2008 TC_3 asteroid (Bischoff et al., 2010; Jenniskens et al., 2009) and the Motopi Pan polymict HED achondrite that is connected to the 2018 LA asteroid and likely originated from 4 Vesta (Jenniskens et al., 2021). A detailed study of the terrestrial ages of the three lithologies will be required to ultimately prove if they all fell together as part of an impacting meteoroid in Malotas in 1931.

CONCLUSION

Petrology, chemical compositions, and replicate analyses of oxygen isotopes (in ‰: $\delta^{17}O^*$ of 1.785 and 1.775; $\delta^{18}O$ of 3.779 ± 0.003 and 3.787 ± 0.005; $\Delta^{17}O$ of −0.208 ± 0.006 and − 0.222 ± 0.007) indicate that Malotas (b) is a eucrite. Considering the texture, chemical, and mineral compositions of the constituent mineral phases, this sample represents a monomict basaltic eucrite. The REE and refractory lithophile element abundances display a distinctive Stannern-trend signature. The presence of pyroxenes with augite exsolution as well as the chemical composition of chromite grains provide evidence of at least one thermal metamorphic event, classifying Malotas (b) as a metamorphosed type 4 basaltic eucrite with final equilibration temperatures ranging between 700 and 805 °C.

Similar to other basaltic eucrites, Malotas (b) has textural and mineralogical features that help to decipher the physicochemical secondary processes that affected this rock:

1. A vapor-driven metasomatic alteration process, as judged by the porous nature of silica, could have triggered both the chemical change of plagioclase (i.e., Ca-enrichment) in the secondary veinlets inside large pyroxene grains as well as the breakdown of pyroxene to silica and troilite.
2. A thermal annealing process is inferred by the presence of pockets with granoblastic textures occurring mainly in the FG lithology. Such a recrystallization event took place in conjunction with chemical changes (Ca-enrichment) of plagioclase grains.
3. Finally, a late and mild thermal event as shown by a single, relatively thin, melt vein cross-cutting both FG and CG lithologies took place after Malotas (b) crystallization and brecciation. A late-stage thermal event is consistent with the distinct nominal gas retention ages determined for U/Th-^{4}He and K-Ar (1.2 Ga and ~ 4.0 Ga, respectively, for the eucritic Malotas [b] samples). Brecciation is in line with the presence of solar wind in some but not all Malotas samples measured in this work and reported in the literature.

Despite the very different CRE ages of the three investigated samples (CRE ages from ^{21}Ne used here; Malotas H5, L5 ordinary chondrites, and Malotas [b] basaltic eucrite = 3 Ma, 45–52 Ma, and 27 Ma, respectively), we cannot rule out that the three lithologies could be delivered to the Earth in the same polymict meteoroid body.

Acknowledgments—We thank Dr. Raúl Lira and E. Jawerbaum for kindly providing the samples. We acknowledge the handling of J. Trigo Rodriguez (A.E.) and the thorough review from P. Warren helped considerably to improve the manuscript. Laser ablation analyses are supported by the NASA Emerging Worlds program (80NSSC18K0595, MH). The National High Magnetic Field Laboratory is supported by the National Science Foundation through NSF/DMR-1644779 and the State of Florida. This work has partially been carried out within the framework of the NCCR PlanetS supported by the Swiss National Science Foundation under grants 51NF40_182901 and 51NF40_205606. M.E.I.R. and H.B. acknowledge the financial support of the SNSF. Financial support was also received from Agencia (PICT 1562) and SECITI, Argentina.

Data Availability Statement—Data available in article supplementary material.

Editorial Handling—Dr. Josep M. Trigo-Rodríguez

REFERENCES

Alexeev, V. A. 1998. Parent Bodies of L and H Chondrites: Times of Catastrophic Events. *Meteoritics & Planetary Science* 33: 145–52.

Andersen, D. J., Lindsley, D., and Davidson, P. M. 1993. QUILF: A PASCAL Program to Assess Equilibria Among Fe-Mg-Mn-Ti Oxides, Pyroxenes, Olivine, and Quartz. *Computers and Geosciences* 19: 1333–50.

Barrat, J., Blichert-Toft, J., Gillet, P., and Keller, F. 2000. The Differentiation of Eucrites: The Role of In Situ Crystallization. *Meteoritics & Planetary Science* 35: 1087–100.

Barrat, J. A., Jambon, A., Bohn, M., Blichert-Toft, J., Sautter, V., Göpel, C., Gillet, P., Boudouma, O., and Keller, F. 2003. Petrology and Geochemistry of the Unbrecciated Achondrite Northwest Africa 1240 (NWA 1240): An HED Parent Body Impact Melt. *Geochimica et Cosmochimica Acta* 67: 3959–70.

Barrat, J. A., Yamaguchi, A., Bunch, T. E., Bohn, M., Bollinger, C., and Ceuleneer, G. 2011. Possible Fluid–Rock Interactions on Differentiated Asteroids Recorded in Eucritic Meteorites. *Geochimica et Cosmochimica Acta* 75: 3839–52.

Barrat, J. A., Yamaguchi, A., Greenwood, R. C., Bohn, M., Cotton, J., Benoit, M., and Franchi, I. A. 2007. The Stannern Trend Eucrites: Contamination of Main Group Eucritic Magmas by Crustal Partial Melts. *Geochimica et Cosmochimica Acta* 71: 4108–24.

Beck, A. W., and McSween, H. Y. J. 2010. Diogenites as Polymict Breccias Composed of Orthopyroxenite and Harzburgite. *Meteoritics & Planetary Science* 45: 850–72.

Binzel, R. P., and Xu, S. 1993. Chips Off of Asteroid 4 Vesta: Evidence for the Parent Body of Basaltic Achondrite Meteorites. *Science* 260: 186–91.

Bischoff, A., Horstmann, M., Pack, A., Laubenstein, M., and Haberer, S. 2010. Asteroid 2008 TC3-Almahata Sitta: A Spectacular Breccia Containing Many Different Ureilitic and Chondritic Lithologies. *Meteoritics & Planetary Science* 45: 1638–56.

Bland, P. A., Spurný, P., Towner, M. C., Bevan, A. W. R., Singleton, A. T., Bottke, W. F., Greenwood, R. C., et al. 2009. An Anomalous Basaltic Meteorite from the Innermost Main Belt. *Science* 325: 1525–7.

Buchanan, P. C., Lindstrom, D. J., Mittlefehldt, D. W., Koeberl, C., and Reimold, W. U. 2000. The South African Polymict Eucrite Macibini. *Meteoritics & Planetary Science* 35: 1321–31.

Buchanan, P. C., and Mittlefehldt, D. W. 2003. Lithic Components in the Paired Howardites EET 87503 and EET 87513: Characterization of the Regolith of 4 Vesta. *Antarctic Meteorite Research* 16: 128–51.

Busemann, H., Baur, H., and Wieler, R. 2000. Primordial Noble Gases in "Phase Q" in Carbonaceous and Ordinary Chondrites Studied by Closed-System Stepped Etching. *Meteoritics & Planetary Science* 35: 949–73.

Chen H. Y., Miao B. K., and Huang L. L. 2015. Ancient Silicification on Asteroid 4 Vesta: Evidence from a Eucrite Grove Mountains (GRV) 13001 from Antarctic (Abstract #5003). 78th Meeting of the Meteoritical Society.

Consolmagno, G. J., and Drake, M. J. 1977. Composition and Evolution of the Eucrite Parent Body: Evidence from Rare Earth Elements. *Geochimica and Cosmochimica Acta* 41: 1271–82.

Cressy, P. J., Jr., and Bogard, D. D. 1976. On the Calculation of Cosmic-Ray Exposure Ages of Stone Meteorites. *Geochimica and Cosmochimica Acta* 40: 749–62.

Di Gregorio, M., Busemann, H., Hunt, A. C., Krietsch, D., Schönbächler, M., and Maden, C. 2019. Variable Cosmogenic Argon in L/LL5 Chondrite Knyahinya (Abstract #6384). Annual Meeting of the Meteoritical Society.

Drake, M. J. 2001. The Eucrite/Vesta Story. *Meteoritics & Planetary Science* 36: 501–13.

Duke, M. B., and Silver, L. T. 1967. Petrology of Eucrites, Howardites and Mesosiderites. *Geochimica and Cosmochimica Acta* 31: 1637–42.

Eugster, O. 1988. Cosmic-Ray Production-Rates for ^{3}He, ^{21}Ne, ^{38}Ar, ^{83}Kr, and ^{126}Xe in Chondrites Based on 81Kr-Kr Exposure Ages. *Geochimica and Cosmochimica Acta* 52: 1649–62.

Eugster, O., and Michel, T. 1995. Common Asteroid Break-Up Events of Eucrites, Diogenites, and Howardites and Cosmic-Ray Production Rates for Noble Gases in Achondrites. *Geochimica and Cosmochimica Acta* 59: 177–99.

Goodrich, C. A., Zolensky, M. E., Fioretti, A. M., Shaddad, M. H., Downes, H., Hiroi, T., Kohl, I., et al. 2019. The First Samples from Almahata Sitta Showing Contacts Between Ureilitic and Chondritic Lithologies: Implications for the Structure and Composition of Asteroid 2008 TC_3. *Meteoritics & Planetary Science* 54: 2769–813.

Greenwood, R. C., Burbine, T. H., Miller, M. F., and Franchi, I. A. 2017. Melting and Differentiation of Early-Formed Asteroids: The Perspective from High Precision Oxygen Isotope Studies. *Chemie der Erde-Geochemistry* 77: 1–43.

Greenwood, R. C., Franchi, I. A., Jambon, A., and Buchanan, P. C. 2005. Widespread Magma Oceans on Asteroidal Bodies in the Early Solar System. *Nature* 435: 916–8.

Haba, M. K., Yamaguchi, A., Horie, K., and Hidaka, H. 2014. Major and Trace Elements of Zircons from Basaltic Eucrites: Implications for the Formation of Zircons on the Eucrite Parent Body. *Earth and Planetary Science Letters* 387: 10–21.

Herzog, G. F., and Caffee, M. W. 2014. 1.13—Cosmic-Ray Exposure Ages of Meteorites. In *Treatise on Geochemistry, 2nd ed*, edited by H. D. Holland, and K. K. Turekian, 419–54. Oxford: Elsevier.

Hess, H. H., and Henderson, E. P. 1949. The Moore County Meteorite: A Further Study with Comment on Its Primordial Environment. *American Mineralogist* 34: 494–507.

Huss, G. R., and Lewis, R. S. 1994. Noble Gases in Presolar Diamonds I: Three Distinct Components and Their Implications for Diamond Origins. *Meteoritics* 29: 791–810.

Iizuka, T., Yamaguchi, A., Haba, M. K., Amelin, Y., Holden, P., Zink, S., Huyskens, M. H., and Ireland, T. R. 2015. Timing of Global Crustal Metamorphism on Vesta as Revealed by High-Precision U-Pb Dating and Trace Element Chemistry of Eucrite Zircon. *Earth and Planetary Science Letters* 409: 182–92.

Jenniskens, P., Gabadirwe, M., Yin, Q. Z., Proyer, A., Moses, O., Kohout, T., Franchi, F., et al. 2021. The Impact and Recovery of Asteroid 2018 LA. *Meteoritics & Planetary Science* 56: 844–93.

Jenniskens, P., Shaddad, M. H., Numan, D., Elsir, S., Kudoda, A. M., Zolensky, M. E., Le, L., et al. 2009. The Impact and Recovery of Asteroid 2008 TC(3). *Nature* 458: 485–8.

Jolliff, B. L., Hughes, J. M., Freeman, J. J., and Ziegler, R. A. 2006. Crystal Chemistry of Lunar Merrillite and

Comparison to Other Meteoritic and Planetary Suites of Whitlockite and Merrillite. *American Mineralogist* 91: 1583–95.

Jones, R. H., McCubbin, F. M., Dreeland, L., Guan, Y., Burger, P. V., and Shearer, C. K. 2014. Phosphate Minerals in LL Chondrites: A Record of the Action of Fluids During Metamorphism on Ordinary Chondrite Parent Bodies. *Geochimica et Cosmochimica Acta* 132: 120–40.

Kagami, S., Haba, M. K., Yokoyama, T., Usui, T., and Greenwood, R. C. 2019. Geochemistry and Sm-Nd Chronology of a Stannern-Group Eucrite, Northwest Africa 7188. *Meteoritics & Planetary Science* 54: 2710–28.

Karner, J., Papike, J. J., and Shearer, C. K. 2003. Olivine from Planetary Basalts: Chemical Signatures That Indicate Planetary Parentage and Those That Record Igneous Setting and Process. *American Mineralogist* 88: 806–16.

Lee, J. Y., Marti, K., Severinghaus, J. P., Kawamura, K., Yoo, H. S., Lee, J. B., and Kim, J. S. 2006. A Redetermination of the Isotopic Abundances of Atmospheric Ar. *Geochimica and Cosmochimica Acta* 70: 4507–12.

Liao, S. Y., and Hsu, W. B. 2017. The Petrology and Chronology of NWA 8009 Impact Melt Breccia: Implication for Early Thermal and Impact Histories of Vesta. *Geochimica et Cosmochimica Acta* 204: 159–78.

Lingner, D. W., Huston, T. J., Hutson, M., and Lipschutz, M. E. 1987. Chemical Studies of H Chondrites. I: Mobile Trace Elements and Gas Retention Ages. *Geochimica et Cosmochimica Acta* 51: 727–39.

Llorca, J., Casanova, I., Trigo-Rodriguez, J. M., Madiedo, J. M., Roszjar, J., Bischoff, A., Ott, U., Franchi, I., Greenwood, R., and Laubenstein, M. 2009. The Puerto Lápice Eucrite. *Meteoritics & Planetary Science* 44: 159–74.

Lodders, K., and Fegley, B. 1998. *The Planetary Scientist's Companion*. New York: Oxford University Press.

Mamyrin, B. A., Anufriyev, G. S., Kamenskii, I. L., and Tolstikhin, I. N. 1970. Determination of the Isotopic Composition of Atmospheric Helium. *Geochemical International* 7: 498–505.

Mason, B. 1962. *Meteorites*. New York: Wiley.

Mason, B. 1963. The Hypersthene Achondrites. *American Museum Novitates* 2155: 13.

Mayne, R. G., McSween, H. Y. Jr, McCoy, T. J., and Gale, A. 2009. Petrology of the Unbrecciated Eucrites. *Geochimica et Cosmochimica Acta* 73: 794–19.

Mayne, R. G., Smith, S. E., and Corrigan, C. M. 2016. Hiding in the Howardites: Unequilibrated Eucrite Clasts as a Guide to the Formation of Vesta's Crust. *Meteoritics & Planetary Science* 51: 2387–402.

McCarthy, T. S., Erlank, A. J., and Willis, J. P. 1973. On the Origin of Eucrites and Diogenites. *Earth and Planetary Science Letters* 18: 433–42.

McCord, T. B., Adams, J. B., and Johnson, T. V. 1970. Asteroid Vesta: Spectral Reflectivity and Compositional Implications. *Science* 168: 1445–7.

McCubbin, F. M., Shearer, C. K., Burger, P. V., Hauri, E. H., Wang, J., Elardo, S. M., and Papike, J. J. 2014. Volatile Abundances of Coexisting Merrillite and Apatite in the Martian Meteorite Shergotty: Implications for Merrillite in Hydrous Magmas. *American Mineralogist* 99: 1347–54.

McSween, H. Y., Binzel, R. P., De Sanctis, M. C., Ammannito, E., Prettyman, T. H., Beck, A. W., Reddy, V., et al. 2013. Dawn; the Vesta–HED Connection; and the Geologic Context for Eucrites, Diogenites, and Howardites. *Meteoritics & Planetary Science* 48: 2090–104.

McSween, H. Y., Mittlefehldt, D. W., Beck, A. W., Mayne, R. G., and McCoy, T. J. 2011. HED Meteorites and Their Relationship to the Geology of Vesta and the Dawn Mission. *Space Science Reviews* 163: 141–74.

Metzler, K., Bobe, K., Palme, H., Spettel, B., and Stöffler, D. 1995. Thermal and Impact Metamorphism on the HED Parent Asteroid. *Planetary and Space Science* 43: 499–525.

Misawa, K., Yamaguchi, A., and Kaiden, H. 2005. U-Pb and ^{207}Pb-^{206}Pb Ages of Zircons from Basaltic Eucrites: Implications for Early Basaltic Volcanism on the Eucrite Parent Body. *Geochimica et Cosmochimica Acta* 69: 5847–61.

Mittlefehldt, D. W. 1979. Petrographic and Chemical Characterization of Igneous Lithic Clasts from Mesosiderites and Howardites and Comparison with Eucrites and Diogenites. *Geochimica et Cosmochimica Acta* 43: 1917–35.

Mittlefehldt, D. W. 1994. The Genesis of Diogenites and HED Parent Body Petrogenesis. *Geochimica et Cosmochimica Acta* 58: 1537–52.

Mittlefehldt, D. W. 2005. Ibitira: A Basaltic Achondrite from a Distinct Parent Asteroid and Implications for the Dawn Mission. *Meteoritics & Planetary Science* 40: 665–77.

Mittlefehldt, D. W. 2015. Asteroid 4 Vesta: I. The Howardite-Eucrite-Diogenite (HED) Clan of Meteorites. *Chemie der Erde—Geochemistry* 75: 155–83.

Mittlefehldt, D. W., Herrin, J. S., Quinn, J. E., Mertzman, S. A., Cartwright, J. A., Mertzman, K. R., and Peng, Z. X. 2013. Composition and Petrology of HED Polymict Breccias: The Regolith of (4) Vesta. *Meteoritics & Planetary Science* 48: 2105–34.

Mittlefehldt, D. W., and Lindstrom, M. M. 1993. Geochemistry and Petrology of a Suite of Ten Yamato HED Meteorites. *Antarctic Meteorite Research* 6: 268.

Mittlefehldt D. W., McCoy T. J., Goodrich C. A., and Kracher A. 1998. Non-Chondritic Meteorites from Asteroidal Bodies. In *Planetary Materials*, edited by Papike, J. J. Reviews in Mineralogy, Vol. 36. Washington, D.C.: Mineralogical Society of America. 1-195.

Nyquist, L. E., Takeda, H., Bansal, B. M., Shih, C. Y., Wiesmann, H., and Wooden, J. L. 1986. Rb-Sr and Sm-Nd Internal Isochron Ages of a Subophitic Basalt Clast and a Matrix Sample from the Y75011 Eucrite. *Journal of Geophysical Research: Solid Earth* 91: 8137–50.

Olsacher J. 1931. Imprenta de la Universidad, Cordoba, 1–18.

Pang, R.-L., Zhang, A.-C., and Wang, R.-C. 2017. Complex Origins of Silicate Veinlets in HED Meteorites: A Case Study of Northwest Africa 1109. *Meteoritics & Planetary Science* 52: 2113–31.

Papike, J. J. 1981. The Lunar Regolith: Significance of the Chemistry of the <10 μm Fraction and a Model for Agglutinate Formation Involving Fusion of the Finest Fraction (F^3). 12th Lunar and Planetary Science Conference. pp. 805–7.

Papike, J. J. 1998. Comparative Planetary Mineralogy: Chemistry of Melt-Derived Pyroxene, Feldspar and Olivine. In *Planetary Materials*, edited by J. J. Papike, 7-1–7-11. Washington, D.C.: Mineralogical Society of America.

Papike, J. J., Karner, J. M., and Shearer, C. K. 2003. Determination of Planetary Basalt Parentage: A Simple Technique Using the Electron Microprobe. *American Mineralogist* 88: 469–72.

Papike, J. J., Karner, J. M., and Shearer, C. K. 2005. Comparative Planetary Mineralogy: Valence State Partitioning of Cr, Fe, Ti, and V Among Crystallographic Sites in Olivine, Pyroxene, and Spinel from Planetary Basalts. *American Mineralogist* 90: 277–90.

Patiño-Douce, A. E., and Roden, M. F. 2006. Apatite as a Probe of Halogen and Water Fugacities in the Terrestrial Planets. *Geochimica et Cosmochimica Acta* 70: 3173–96.

Patzer, A., and McSween, H. Y. 2018. Ferroan Olivine-Bearing Eucrite Clasts Found in Howardites. *Meteoritics & Planetary Science* 53: 1131–49.

Reddy, V., Le Corre, L., O'Brien, D. P., Nathues, A., Cloutis, E. A., Durda, D. D., Bottke, W. F., Bhatt, M. U., Nesvorny, D., and Buczkowski, D. 2012. Delivery of Dark Material to Vesta Via Carbonaceous Chondritic Impacts. *Icarus* 221: 544–59.

Reid, A. M., and Barnard, B. 1979. Unequilibrated and Equilibrated Eucrites (Abstract #1357). 10th Lunar and Planetary Science Conference. pp. 1019–24.

Riebe, M. E. I., Welten, K. C., Meier, M. M. M., Wieler, R., Barth, M. I. F., Ward, D., Laubenstein, M., et al. 2017. Cosmic-Ray Exposure Ages of Six Chondritic Almahata Sitta Fragments. *Meteoritics & Planetary Science* 52: 2353–74.

Rombeck, S., Vollmer, C., Roszjar, J., Sarafian, A. R., and Klemme, S. 2021. How Do Secondary Iron Enrichments Form Within Basaltic Eucrites? An Experimental Approach. *Meteoritics & Planetary Science* 56: 911–28.

Roszjar, J. 2019. Secondary Alteration of the Serra Pelada Eucrite. *Meteoritics & Planetary Science* 54: A6311.

Roszjar, J., Metzler, K., Bischoff, A., Barrat, J. A., Geisler, T. G., Greenwood, R. C., Franchi, I. A., and Klemme, S. 2011. Thermal History of Northwest Africa 5073—A Coarse Grained Stannern-Trend Eucrite Containing cm-Sized Pyroxenes and Large Zircon Grains. *Meteoritics & Planetary Science* 46: 1754–73.

Roszjar, J., Whitehouse, M. J., and Bischoff, A. 2014. Meteoritic Zircon—Occurrence and Chemical Characteristics. *Chemie der Erde—Geochemistry* 74: 453–69.

Roszjar, J., Whitehouse, M. J., Srinivasan, G., Mezger, K., Scherer, E. E., Van Orman, J. A., and Bischoff, A. 2016. Prolonged Magmatism on 4 Vesta Inferred from Hf-W Analyses of Eucrite Zircon. *Earth and Planetary Science Letters* 452: 216–26.

Russell, C. T., Raymond, C. A., Coradini, A., McSween, H. Y., Zuber, M. T., Nathues, A., and Titus, T. N. 2012. Dawn at Vesta: Testing the Protoplanetary Paradigm. *Science* 336: 684–6.

Saavedra, M. E., Roszjar, J., Humayun, M., Tanaka, R., Varela, M. E., and Lira, R. 2019. Malotas: A New View of an Old Fall from Argentina. 82nd Annual Meeting of The Meteoritical Society, Abstract #6168.

Sarafian, A. R., John, T., Roszjar, J., and Whitehouse, M. J. 2017. Chlorine and Hydrogen Degassing in Vesta's Magma Ocean. *Earth and Planetary Science Letters* 459: 311–9.

Sarafian, A. R., Roden, M. F., and Patiño Douce, A. E. 2013. The Nature of Volatiles in Eucrites: Clues from Apatite. *Meteoritics & Planetary Science* 48: 2135–54.

Schiller, M., Baker, J. A., and Bizzarro, M. 2010. ^{26}Al–^{26}Mg Dating of Asteroidal Magmatism in the Young Solar System. *Geochimica and Cosmochimica Acta* 74: 4844–64.

Schultz, L., Signer, P., Lorin, J. C., and Pellas, P. 1972. Complex Irradiation History of the Weston Chondrite. *Earth and Planetary Science Letters* 15: 403–10.

Schwartz, J. M., and McCallum, I. S. 2005. Comparative Study of Equilibrated and Unequilibrated Eucrites: Subsolidus Thermal Histories of Haraiya and Pasamonte. *American Mineralogist* 90: 1871–86.

Scott, E. R. D., Greenwood, R. C., Franchi, I. A., and Sanders, I. S. 2009. Oxygen Isotopic Constraints on the Origin and Parent Bodies of Eucrites, Diogenites, and Howardites. *Geochimica et Cosmochimica Acta* 73: 5835–53.

Singerling, S. A., Modi, A. L., McFerrin, B., Worsham, E., McSween, H. Y., Rumble, D., Tanaka, R., and Taylor, L. A. 2013. Two New Eucrite Breccias from Northwest Africa. *Meteoritics & Planetary Science* 48: E1–9.

Srinivasan, B. 1977. Noble Gases in Six Ordinary Chondrites: Comparison of Exposure Ages from Noble Gases with ^{26}Al Ages. *Geochimica et Cosmochimica Acta* 41: 977–83.

Stolper, E. 1977. Experimental Petrology of Eucritic Meteorites. *Geochimica et Cosmochimica Acta* 41: 587–611.

Takeda, H. 1991. Comparison of Antarctic and Non-Antarctic Achondrites and Possible Origin of the Differences. *Geochimica et Cosmochimica Acta* 55: 35–47.

Takeda, H., and Graham, A. 1991. Degree of Equilibration of Eucritic Pyroxenes and Thermal Metamorphism of the Earliest Planetary Crust. *Meteoritics* 26: 129–34.

Thomas, P. C., Binzel, R. P., Gaffey, M. J., Storrs, A. D., Wells, E. N., and Zellner, B. H. 1997. Impact Excavation on Asteroid 4 Vesta: Hubble Space Telescope Results. *Science* 277: 1492–5.

Treiman, A. H., Lanzirotti, A., and Xirouchakis, D. 2004. Ancient Water on Asteroid 4-Vesta: Evidence from a Quartz Veinlet in the Serra de Magé Eucrite Meteorite. *Earth and Planetary Science Letters* 219: 189–99.

Vollmer, C., Rombeck, S., Roszjar, J., Sarafian, A. R., and Klemme, S. 2020. The Brecciated Texture of Polymict Eucrites: Petrographic Investigations of Unequilibrated Meteorites from the Antarctic Yamato Collection. *Meteoritics & Planetary Science* 55: 558–74.

Ward, D., Bischoff, A., Roszjar, J., Berndt, J., and Whitehouse, M. J. 2017. Trace Element Inventory of Meteoritic Ca-Phosphates. *American Mineralogist* 102: 1856–80.

Warren, P. H., and Jerde, E. 1987. Composition and Origin of Nuevo Laredo Trend Eucrites. *Geochimica et Cosmochimica Acta* 51: 713–25.

Warren, P. H., Rubin, A. E., Isa, J., Gessler, N., Ahn, I., and Choi, B.-G. 2014. Northwest Africa 5738: Multistage Fluid-Driven Secondary Alteration in an Extraordinarily Evolved Eucrite. *Geochimica et Cosmochimica Acta* 141: 199–227.

Wasson, J. T., and Kallemeyn, G. W. 1988. Compositions of Chondrites. *Philosophical Transactions of the Royal Society of London Series A, Mathematical and Physical Sciences* 325: 535–44.

Welten, K., Caffee, M. W., Franke, L., Jull, A. J. T., LeClerc, M. D., Metzler, K., and Ott, U. 2011. The L3–6 Chondritic Regolith Breccia Northwest Africa (NWA) 869: (II) Noble Gases and Cosmogenic Radionuclides. *Meteoritics & Planetary Science* 46: 970–88.

Wiechert, U. H., Halliday, A. N., Palme, H., and Rumble, D. 2004. Oxygen Isotope Evidence for Rapid Mixing of the HED Meteorite Parent Body. *Earth Planetary Science Letters* 221: 373–82.

Wieler, R. 2002. Cosmic-Ray-Produced Noble Gases in Meteorites. In *Noble Gases in Geochemistry and*

Cosmochemistry, Reviews in Mineralogy and Geochemistry, edited by D. Porcelli, C. J. Ballentine, and R. Wieler, Vol. 47. Washington D.C.: Mineralogical Society of America. 125–70.

Wieler, R., Graf, T., Pedroni, A., Signer, P., Pellas, P., Fieni, C., Suter, M., Vogt, S., Clayton, R. N., and Laul, J. C. 1989. Exposure History of the Regolithic Chondrite Fayetteville: II. Solar-Gas-Free Light Inclusions. *Geochimica and Cosmochimica Acta* 53: 1449–59.

Yamaguchi, A. 2000. Spinels in Basaltic Eucrites: Implication for Crystallization and Metamorphic History (Abstract). *Meteoritics & Planetary Science* 35: A174.

Yamaguchi, A., Barrat, J. A., Greenwood, R. C., Shirai, N., Okamoto, C., Setoyanagi, T., Ebihara, M., Franchi, I. A., and Bohn, M. 2009. Crustal Partial Melting on Vesta: Evidence from Highly Metamorphosed Eucrites. *Geochimica et Cosmochimica Acta* 73: 7162–82.

Yamaguchi, A., Clayton, R. N., Mayeda, T. K., Ebihara, M., Oura, Y., Miura, Y. N., Haramura, H., Misawa, K., Kojima, H., and Nagao, K. 2002. A New Source of Basaltic Meteorites Inferred from Northwest Africa 011. *Science* 296: 334–6.

Yamaguchi, A., Taylor, G. J., and Keil, K. 1996. Global Crustal Metamorphism of the Eucrite Parent Body. *Icarus* 124: 97–112.

Zähringer, J. 1966. Chronology of Chondrites with Rare Gas Isotopes. *Meteoritika* 27: 25–40.

Zhang, A., and Yurimoto, H. 2013. Petrography and Mineralogy of the Ungrouped Type 3 Carbonaceous Chondrite Dar al Gani 978. *Meteoritics & Planetary Science* 48: 1651–77.

Zhang, A.-C., Wang, R.-C., Hsu, W.-B., and Bartoschewitz, R. 2013. Record of S-Rich Vapors on Asteroid 4 Vesta: Sulfurization in the Northwest Africa 2339 Eucrite. *Geochimica et Cosmochimica Acta* 109: 1–13.

Zhou, Q., Yin, Q. Z., Young, E. D., Li, X. H., Wu, F. Y., Li, Q. L., Liu, Y., and Tang, G. Q. 2013. SIMS Pb–Pb and U-Pb Age Determination of Eucrite Zircons at <5 μm Scale and the First 50 Ma of the Thermal History of Vesta. *Geochimica et Cosmochimica Acta* 110: 152–75.

Zucolotto, M. E., Tosi, A. A., Villaça, C. V. N., Moutinho, A. L. R., Andrade, D. P. P., Faulstich, F., Gomes, A. M. S., Rios, D. C., and Rocha, M. C. 2018. Serra Pelada: The First Amazonian Meteorite Fall Is a Eucrite (Basalt) from Asteroid 4-Vesta. *Anais da Academia Brasileira de Ciências* 90: 3–16.

SUPPORTING INFORMATION

Additional supporting information may be found in the online version of this article.

Data S1. Detailed description of the analytical techniques and methods used to characterize the Malotas (b) sample. This section provides a summary and overview of the techniques applied.

Data S2. Copy of Prof. Olsacher's paper, entitled: The meteorite of Salavina, 1931.

Fig. S1. Some characteristic petrological features in Malotas (b) as observed with the SEM in BSE mode (A) and by applying superimposed EDS elemental maps (B–F). (B–D) Characteristic Cpx exsolution lamellae (bluish Ca enrichments) in large (red Mg–rich) Opx crystals due to thermal metamorphism are observed, together with anorthitic plagioclase veinlets (Al–rich green) cross–cutting the grains. Note that the plagioclase veinlets are more abundant and larger in size towards the Opx crystal cores. (D) One large shock melt vein (MV), more enriched in Al and Ca (Pl–component) and cross–cutting through the whole sample is outlined. (E) Detail of a recrystallized area containing abundant accessory phases such as ilmenite (Ti lighter blue), Ca–phosphates (F–apatite an merrillite, pinkish), sulfides (FeS yellow). (F) Typical texture of the fine–grained lithology manila composed of coexisting Opx and Cpx (Ca–rich dark blue) and plagioclase (green) with some accessory phases (P, Ti, S–enriched crystals).

Table S1. Electron microprobe analysis of minerals in the coarse-grained portion of Malotas (b) eucrite. Uncertainties of endmember compositions are 1σ.

Table S2. Electron microprobe analysis of minerals in the fine-grained portion of Malotas (b) eucrite. Uncertainties of endmember compositions are 1σ.

Table S3. Major and trace element compositions determined by laser ablation ICP-MS of fine-grained, coarse-grained, and bulk of Malotas (b). Oxides in wt%, trace elements in μg g^{-1}.

Table S4. Geothermometry data used for QUILF program and estimated temperatures for Malotas (b).

Table S5. Concentrations (in 10^{-8} cm^3 g^{-1}) and isotopic compositions of He and Ne.

Table S6. The isotopic composition of Xe in ×100.

Table S7. The isotopic composition of Kr in ×100.

Table S8. Concentrations of Ar (in 10^{-8} cm^3 g^{-1}) and of Kr, Xe (in 10^{-10} cm^3 g^{-1}) and isotopic composition of Ar.

Table S9. The concentrations of cosmogenic ^{3}He, ^{21}Ne, and ^{38}Ar (in 10^{-8} cm^3 g^{-1}) and production rates (P[3], P[21], P[38]) calculated using Eugster and Michel (1995) for the eucrite and Eugster (1988) for the ordinary chondrites in 10^{-8} cm^3 (g $Myr)^{-1}$. Resulting CRE ages (T[3], T[21], T[38]) are given in Myr and as ranges when variation in production rates or measurement uncertainties was significant.

Table S10. The concentration of radiogenic ^{4}He, ^{40}Ar measured, and ^{40}Ar corrected assuming the trapped component (only detected in the ordinary chondrites) to be air (in 10^{-8} cm^3/g^{-1}) and the resulting nominal (U-Th)/He and K-Ar ages.